The Dissertation Committee for Cynthia Simeonova Trendafilova
certifies that this is the approved version of the following dissertation:

Extensions of the Standard Model with Relation to Dark Matter and Flavor Structure

Committee:

_____

Can Kilic, Supervisor

_____

Jacques Distler

_____

Willy Fischler

_____

Sonia Paban

_____

Paul Shapiro

Extensions of the Standard Model with Relation to Dark Matter and Flavor Structure

by

Cynthia Simeonova Trendafilova

Dissertation

Presented to the Faculty of the Graduate School of

The University of Texas at Austin

in Partial Fulfillment

of the Requirements

for the degree of

Doctor of Philosophy

The University of Texas at Austin

August 2019

Dedicated to Kimi and Cali.

Acknowledgements

I would like to thank the following people:

Extensions of the Standard Model with Relation to Dark Matter and Flavor Structure

Publication No. _____

Cynthia Simeonova Trendafilova, Ph.D.
The University of Texas at Austin, 2019

Supervisors: Can Kilic

There is a great deal of observational evidence now suggesting the existence of dark matter as the major constituent of the matter content in our universe. Its nature and particle content are still a mystery, and proposing suitable models that can explain its properties would be of great value. This dissertation is a study of the phenomenology of dark matter models with a focus on flavor structure and the rich consequences it can have for the dark sector. We give three implementations of flavored dark matter (FDM) and discuss interesting phenomenological and observational consequences of each. The first model contains asymmetric lepton-flavored dark matter alongside a Higgs portal interaction, resulting in destructive interference that significantly weakens constraints from direct detection bounds. The second study implements a model where a present-day FDM relic can be symmetric, even though it was initially produced in the early universe with an asymmetry in each flavor transferred from the Standard Model via its FDM interactions. Finally, we explore a model where asymmetric DM components interacting via a long-range force can combine to form bound states, and the interactions between these components and a dark photon can address several outstanding issues from astrophysical observations.

Contents

List of Figures

Chapter One: Introduction

1.1 The Standard Model

The Standard Model (SM) of particle physics describes the interactions and particles which we have observed to govern and constitute our universe. The electroweak and strong forces, along with the various particles which participate in these interactions, are described by this model, and their parameters have been observed and characterized through our various particle physics experiments, including our recent observations at the Large Hadron Collider (LHC).

- The SM has the gauge symmetry $SU(3)_C \times SU(2)_L \times U(1)_Y$, or color, weak isospin, and hypercharge. There are also the corresponding gauge fields: the gluons, G_a, and the electroweak bosons, W_b and B.

- The fermionic matter content of the SM includes three copies, or "flavors," of each of the fermion fields: the left- and right-handed leptons, L_i and e_i^c; the left-handed quarks, Q_i; and the up- and down-type right-handed quarks, u_i^c d_i^c.

- The Higgs boson, ϕ, is a spin 0 boson whose VEV breaks the gauge symmetry to $SU(3) \times U(1)_{EM}$ and gives masses to the fermions.

In addition to the Standard Model, the general theory of relativity is the cornerstone describing the gravitational interactions between matter and spacetime, although it has not yet been satisfactorily combined within the quantum field theoretical structure of the Standard Model. In spite of the experimental successes of both of these theories and the precision to which they have been tested, and aside from the issue of unifying the two ideas, there are still other features within the Standard Model which have not been successfully explained and are currently active areas of research.

1.2 Questions of the Standard Model

In this section we outline some oustanding issues with the Standard Model which we aim to connect with the dark matter models presented in this thesis.

1.2.1 Flavor

As stated in the previous section, there are three flavors of each quark and lepton in the Standard Model. There is an approximate global $U(3)^5$ symmetry, broken only by the presence of the Yukawa matrices which describe the interactions between the fermions and the Higgs [1]:

$$\mathcal{L}_Y = -Y_{ij}^d \overline{Q_i} \phi d_j^c - Y_{ij}^u \overline{Q_i} \tilde{\phi} u_j^c - Y_{ij}^e \overline{L_i} \phi e_j^c + \text{h.c.}. \tag{1.1}$$

Although total baryon and lepton numbers are conserved, they are not conserved on an individual flavor-by-flavor basis. Flavor-changing interactions among the leptons are governed by the parameters of the Pontecorvo-Maki-Nakagawa-Sakata matrix (PMNS matrix), and likewise for the quarks by the Cabibbo-Kobayashi-Maskawa matrix (CKM matrix). The Yukawa couplings and thus the masses among the different fermion generations are also quite different; for example, among the quarks, they vary from 2.2 MeV for the up quark to 173 GeV for the top quark. Why this flavor structure exists is unknown, and although we can observe and measure the numerical values of these parameters, we do not know what mechanism can explain and predict them. Any new theories developed to address physics beyond the Standard Model may hope to tie into the flavor puzzle in some way, and we might expect new matter constituents to exhibit similar structures among their fields and parameters.

1.2.2 Asymmetry

Another open question regarding the matter content of the Standard Model is the issue of the observed baryon asymmetry. The field content of the SM includes both particles and anti-particles for the baryons, and we might expect the universe to be symmetric in its populations of both types of matter. Observationally, however, the universe is dominated by only one of these components (which we conventionally call matter), and we observe no significant presence of antibaryons. The observed baryon

asymmetry today has been measured as [2]:

$$5.8 \times 10^{-10} \leq \eta \leq 6.6 \times 10^{-10}, \tag{1.2}$$

where

$$\eta = \frac{n_B - n_{\bar{B}}}{n_\gamma}. \tag{1.3}$$

There are several requirements, known as the Sakharov conditions, that need to be met in order to generate an asymmetry among the baryons: baryon number violation, C and CP violation, and dynamics that are occurring out of equilibrium [3]. Electroweak sphalerons can break B-number while conserving $B - L$, and although there are sources of CP violation within the Standard Model as parametrized in the CKM matrix, it is not sufficient to generate an asymmetry of the observed magnitude. Thus some new physics must be introduced in order to explain how this baryon asymmetry could have been generated, and any new sectors added in these theories can have asymmetries among their constituents which may share a common origin with those in the SM.

1.2.3 Dark matter

Decades' worth of astrophysical and cosmological observations are now consistently hinting at the presence of additional matter components beyond the known particle content of the Standard Model. Several different observational avenues, including galaxy rotation curves and gravitational lensing, give results which are inconsistent with the quantity of visible matter that we observe. This suggests either a flaw in our understanding of gravitational interactions, or the presence of new, unknown particles. There have been attempts to modify gravity to explain these observations, but they have difficulty being consistent across all scales, and another possibility is that there is simply some new matter content beyond the SM. These new particles interact with SM matter gravitationally as observed, but they do not seem to interact noticably via the gauge interactions of the Standard Model; terrestrial experiments to detect the scattering of dark matter (DM) from SM nuclei have so far provided only null results. Dark matter may interact with itself, but there are some observational limits on the strength of such interactions. Given our limited knowledge aside from its gravitational presence, the content, properties, and origin of DM — which is observed to make up approximately 85% of the matter content in our universe — are

all unknown and remain one of the biggest mysteries in modern theoretical physics. Addressing this issue is an interesting challenge in its own right, but working to tie it into some of the open puzzles in the Standard Model can provide additional motivation for our theories.

1.3 ΛCDM

In addition to identifying the particle building blocks of our universe and the forces that govern their interactions, another area in modern theoretical physics is cosmology, addressing the question of how our universe formed and developed over time. The current dominant cosmological model which does a good job of describing several main aspects of our observations is the Lambda Cold Dark Matter (ΛCDM) model. There are three major components included in this model:

- Ordinary matter – This is as we know it from the Standard Model, described in section 1.1.

- Cosmological constant (Λ) – This describes the presence of dark energy, which is necessary to address the observed accelerated expansion of our universe. Its origin remains unknown and it is currently a measured parameter in the ΛCDM model.

- Cold dark matter (CDM) – As described in section 1.2, the presence of dark matter appears to be necessary to explain many astrophysical observations. There are several restrictions on the properties that viable DM models must meet, including getting the right relic density to match observations, evading current direct detection constraints, and remaining consistent with observations about Big Bang nucleosynthesis (BBN) and stellar evolution. In addition to this, in order to allow for the formation of large-scale structure, DM is expected to be nonrelativistic — though some subcomponent of the DM may be relativistic, the majority of it is thought to be "cold."

As with the Standard Model, in spite of the successes of ΛCDM in explaining observations of the CMB, large-scale structure (LSS), and BBN, there are some obvious issues in the fact that the nature of dark matter and dark energy are still unknown.

There are also other open astrophysical questions which one might hope to address using a DM model with suitable properties.

- The Hubble constant, H_0, tells us the current expansion rate of our universe. Recent cosmological measurements indicate a discrepancy between the value of H_0 observed from local measurement when compared with the value that is inferred from the CMB. One way of potentially addressing the tension is to have a model with extra relativistic degrees of freedom.

- In a similar problem, the σ_8 parameter, which describes the amplitude of the matter power spectrum on the scale of $8h^{-1}$Mpc, gives a different inferred value from early measurements than that from direct, low-redshift measurements. Adding an interacting component in the dark sector can suppress the matter spectrum enough to resolve this discrepancy.

In creating models to address the need for DM, one can incorporate these outstanding questions along with including features related to the SM problems listed in section 1.2.

1.4 Components of this thesis

There have been many proposed DM models incorporating flavored dark matter, where similarly to the Standard Model, the dark fields can come in multiple copies. The DM may then couple to the SM via various channels, and its flavors may correspond to SM flavors, depending on the nature of these interactions. In Chapter 2, we present specifically a model of lepton-flavored dark matter, combined with an asymmetric relic density in the dark sector, which can relieve the tension with bounds from dark matter direct detection experiments. In flavored dark matter models, dark matter can scatter off of nuclei through Higgs and photon exchange, both of which can arise from renormalizable interactions and individually lead to strong constraints from direct detection. While these two interaction channels can destructively interfere in the scattering amplitude, for a thermal relic with equal abundances for the dark matter particle and its antiparticle, this produces no effect on the total event rate. Focusing on lepton-flavored dark matter, we show that it is quite natural for dark matter to have become asymmetric during high-scale leptogenesis, and that in this

case the direct detection bounds can be significantly weakened due to interference. We quantify this by mapping out and comparing the regions of parameter space that are excluded by direct detection for the symmetric and asymmetric cases of lepton-flavored dark matter. In particular, we show that the entire parameter region except for a narrow Higgs resonance window is ruled out in the symmetric case for fermion dark matter when the coupling to the Higgs dominates over the coupling to leptons, while large portions of parameter space are still allowed for the asymmetric case. The same is also true for a dark matter mass above 8 GeV for scalar dark matter when the coupling to leptons dominates over the coupling to the Higgs.

We continue exploring the phenomenological consequences of having flavored and asymmetric dark matter in Chapter 3, in a mechanism we refer to as Secretly Asymmetric Dark Matter (SADM). In this case the dark matter number density today arises from asymmetries generated in individual flavors in the early universe by being transferred from the lepton sector, even though total dark matter number remains zero throughout the history of the universe. If there is a mass splitting between flavors and the heavier ones can decay to the lighest one, it is possible that the dark matter population today is completely symmetric, but with annihilation rates above those expected from thermal WIMPs. We give a simple example of this mechanism using a benchmark model of flavored dark matter. We then discuss the experimental signatures of this setup, which arise mainly from the sector that annihilates the symmetric component of the dark matter; several examples are given for how this might be achieved.

Finally, one may hope that DM models can be used to address some of the currently oustanding puzzles we face from astrophysical and cosmological observations, as discussed in section 1.3. To this end, in Chapter 4 we present a simple model of dark matter that can address these puzzles across a wide range of scales. The model is an application of the SADM mechanism, where several flavors of dark matter are fully asymmetric despite an exact dark matter number symmetry $U(1)_\chi$. The dark matter relic abundance arises from these asymmetries, generated in the early universe through right-handed neutrino decays. The $U(1)_\chi$ is gauged by a massless dark photon, and asymmetries with opposite signs in the different DM flavors result in the formation of bound states. Dark acoustic oscillations in the early universe lead to a suppression in the matter power spectrum for addressing the σ_8 problem. The dark photon as a relativistic degree of freedom contributes to ΔN_{eff}, easing the ten-

sion between the CMB and late-time H_0 measurements. Finally, scattering between the bound states after structure formation leads to a flattening of the dark matter distribution at the cores of haloes.

Chapter Two: Lepton-flavored asymmetric dark matter and interference in direct detection[1]

The steady improvement in the sensitivity of direct detection searches is putting severe constraints on the parameter space of dark matter (DM) models belonging to the weakly interacting massive particle (WIMP) paradigm. These bounds can be relaxed in certain classes of models, including Majorana fermion DM where only spin-dependent scattering contributes, inelastic DM [5, 6, 7] where the observed event rate is severely reduced due to the energy cost of upscattering, or isospin violating DM[8, 9] where destructive interference can occur between the scattering of DM off of protons and neutrons, among others. The idea of destructive interference in the scattering amplitude has been used in several dark matter models in the past [10, 11, 12, 13, 14, 15, 16, 17, 18, 19]. A simple class of models that can give rise to interference is when the DM particle interacts with nuclei via multiple mediators. A nontrivial check in such models is whether the parameters of the model need to be fine-tuned, or in other words, whether scattering amplitudes for the exchange of the mediators are naturally of the same size for generic values of the couplings in the model.

In this chapter we argue that flavored dark matter (FDM) models [20, 21, 22, 23, 24, 25, 26, 27, 28, 29, 30] can give rise to interference in the scattering amplitude quite naturally. These models admit renormalizable couplings between the DM and SM fields that lead to both tree-level Higgs exchange as well as loop-level photon exchange channels for direct detection, with comparable sizes.

Unfortunately, interference between spin-0 (Higgs) and spin-1 (photon) mediated channels will not in general help to ease direct detection constraints for WIMPs, which have equal relic abundances for the DM particle χ and its antiparticle $\bar{\chi}$. The amplitude for a spin-0 exchange channel will have the same sign for χ and $\bar{\chi}$, while the amplitude for a spin-1 exchange channel will change sign[2]. Therefore, any destructive

---

[1]This chapter is based on work previously published as ref. [4]. This author contributed to the methodology, calculations, and text of this paper.

[2]In FDM models, χ cannot be a self-conjugate field due flavor constraints. See Sec. 4.1 for details.

interference that occurs for the scattering of χ off of nuclei will unavoidably lead to constructive interference in the scattering of $\bar{\chi}$, and the total scattering rate will be the same as in the absence of any interference.

On the other hand, for asymmetric DM [31, 32, 33, 34, 35, 36, 37], the destructive interference can significantly weaken direct detection constraints. Interestingly, this too can occur readily in FDM models. In this paper we focus on the case of lepton-flavored DM, where we will show that it is very natural for a DM asymmetry to be generated during high-scale leptogenesis [38] (for additional references see reviews on this subject, e.g. [39, 40]). Using lepton-flavored asymmetric DM as our benchmark model, and contrasting with the same model but with a symmetric χ-$\bar{\chi}$ abundance, we will quantify the impact of interference on the region of parameter space that is compatible with the null results of direct detection experiments. In particular, we will show that for the case of fermion dark matter that couples predominantly to the Higgs, the full parameter region in the symmetric case is ruled out due to direct detection except for a narrow Higgs resonance window, while the asymmetric case can be consistent with the bounds due to interference. This is also true for the case of scalar DM that couples predominantly to leptons when the DM mass is above 8 GeV.

The particle content of FDM models includes three copies of the DM particle χ as well as a mediator particle ϕ which makes renormalizable interactions between χ and the standard model (SM) fermions possible. Due to Lorentz invariance, one of χ and ϕ is necessarily a fermion while the other one is a boson. We will study both possibilities for completeness and highlight the similarities as well as the differences between them.

The outline of the chapter is as follows: In Sec. 2.1 we will review the lepton-flavored DM model and describe its general features, before introducing a mechanism by which it can become asymmetric during high-scale leptogenesis. We will go over the direct detection prospects of lepton-flavored DM in Sec. 2.2 and we will map out the excluded regions in the parameter space of the model for both the symmetric and asymmetric cases in section 2.3. We will conclude in Sec. 2.4 and comment on future directions. Detailed formulae related to the calculation of the relic density in the symmetric case and to the scattering amplitude for direct detection can be found in the appendices.

2.1 The Model

The FDM setup has been described in detail in Ref. [23] so we will only give a brief summary here. The DM is taken to be a singlet under the gauge symmetries of the standard model (SM) but it belongs to a multiplet that transforms nontrivially under the flavor symmetries of the SM, which we will denote by χ_i. There is also a mediator particle ϕ which is a flavor singlet, but which carries SM hypercharge. Assuming that the ϕ mass is heavier than at least one of the χ masses, the lightest of the χ_i is rendered stable by a global $U(1)$ under which only the χ_i and ϕ are charged. We will refer to this $U(1)$ as χ-number.

It was shown in Ref. [23] that FDM is compatible with constraints arising from flavor observables in a minimal flavor violation (MFV) [41] setup, such that the SM Yukawa couplings are the only source of flavor violation. With this assumption, the minimal choice in terms of the number of degrees of freedom is for χ_i to be a flavor triplet.

Which SM flavor symmetry χ_i transforms under determines the SM fermions it can couple to at the renormalizable level. For the rest of this paper we will focus our attention on the specific case of lepton-flavored DM, where $\chi_{e,\mu,\tau}$ transform as a triplet under $SU(3)_{e_R}$. As in Ref. [23], we will work with a benchmark model where χ_τ is the lightest state, but the main conclusions of this paper are insensitive to this choice. A renormalizable coupling to the SM fermions requires one of χ and ϕ to be a fermion, and the other to be a scalar. Note that in order to be a triplet under $SU(3)_{e_R}$, χ_i must be complex, so it is either a complex scalar or a Dirac fermion. If the DM is a scalar, the interaction term is

$$\mathcal{L}_{\text{scalar}} \supset \lambda_{ij}\chi_i\bar{\phi}e_{R,j} + \text{h.c.}, \tag{2.1}$$

while for a fermionic DM it has the form

$$\mathcal{L}_{\text{fermion}} \supset \lambda_{ij}\bar{\chi}_i\phi e_{R,j} + \text{h.c.}. \tag{2.2}$$

As discussed in Ref. [23], within the MFV formalism the flavor structure of λ_{ij} is

$$\lambda_{ij} = (\alpha \mathbb{1} + \beta y^\dagger y)_{ij}. \tag{2.3}$$

In order to reduce clutter, we will assume that $\alpha \gg \beta$, such that we can define $\lambda_{ij} \equiv \lambda_\phi \delta_{ij}$. It should be noted however that this is mainly a choice of convenience and that the main conclusions of this paper are not sensitive to this choice.

In the scalar DM case, the only other renormalizable interaction of the dark sector with the SM allowed by the symmetries of the model is a coupling to the Higgs doublet. Including this interaction, the scalar potential can be written as

$$
\begin{aligned}
V_{\text{scalar}} &= \lambda_h(H^\dagger H - \frac{1}{2}v^2)^2 + \mu_{\chi_i}^2 \chi_i^* \chi_i \\
&+ \lambda_{\chi h}\chi_i^*\chi_i H^\dagger H + \lambda_s(\chi_i^*\chi_i)^2.
\end{aligned}
\tag{2.4}
$$

This potential is bounded from below even for $\lambda_{\chi h} < 0$, provided that

$$
\lambda_h > 0, \qquad \lambda_s > 0, \qquad \lambda_h \lambda_s > \frac{1}{4}\lambda_{\chi h}^2.
\tag{2.5}
$$

Note that negative value $\lambda_{\chi h}$ does not present a problem as long as λ_s is positive and large. After electroweak symmetry breaking, the DM inherits a χ-χ-h coupling. This will contribute to direct detection through tree-level Higgs exchange.

In order to study similar phenomenological features in the fermion DM case, we will also include a dimension-5 term in the Lagrangian

$$
\mathcal{L}_{\text{fermion}} \supset -\frac{\kappa}{\Lambda}\bar\chi_i\chi_i H^\dagger H.
\tag{2.6}
$$

To have consistency between the scalar and fermion DM cases, we will adopt a convention such that

$$
\frac{\kappa}{\Lambda} \equiv \frac{\lambda_{\chi h}}{v},
\tag{2.7}
$$

where v is the electroweak scale, and with the understanding that $\lambda_{\chi h}$ is small in the fermionic DM case. In other words, the dimension-5 term is assumed to have arisen by integrating out additional degrees of freedom at the scale Λ (close to TeV scale), such as a heavy SM singlet scalar with couplings to $\bar\chi$-χ, and to the SM Higgs. Note that the scalar potential in this case can also include a renormalizable $|\phi|^2|H|^2$ term, but the presence of this term will have no effect for the rest of the paper, and for this reason we will not dwell on it any further.

Let us now turn our attention to the generation of a χ asymmetry. We will demonstrate this explicitly in the fermion DM case; it is straightforward to implement the same mechanism in the scalar DM case as well. We assume that a primordial lepton asymmetry is generated via the decay of right-handed neutrinos at a high scale within a few orders of magnitude of the scale of grand unification. The right handed

neutrinos N_R couple to the SM leptons through

$$
\begin{aligned}
\mathcal{L}_{\text{lepton}} \;=\;& \frac{1}{2}(M_N)_{ij}\overline{N}^c_{R,i}N_{R,j} \\
& + \left(y^L_{ij}\bar{L}_iHe_{R,j} + y^N_{ij}\bar{L}_i\tilde{H}N_{R,j}\right) + \text{h.c.}, \qquad (2.8)
\end{aligned}
$$

where L_i are the $SU(2)$ doublet SM lepton fields, $\tilde{H} = \epsilon H^*$ and the first term is a Majorana mass for the right-handed neutrinos. The mechanism by which nonthermal decays of the right-handed neutrinos generate a nonzero lepton asymmetry, and later a nonzero baryon asymmetry through sphaleron processes, is well known (see [39, 40] and references therein). This mechanism relies on CP violating phases in the cross-terms between the tree-level and one-loop contributions to the amplitude for N_R decay.

At first, it may seem that the interaction of Eq. 2.2 is sufficient to transfer any lepton asymmetry generated in the decays of N_R to the χ_i. However, χ-number is still an exact symmetry at this point, which makes it impossible to generate a χ asymmetry from an asymmetry in a different species with no χ-number. Therefore, the crucial ingredient for transferring the lepton asymmetry into the DM sector is breaking χ-number (down to $\mathbb{Z}_2$ such that the stability of DM is not lost). For this purpose we add one more degree of freedom to the model, a *real* scalar field S, with the interaction

$$
\mathcal{L}_S = y^S_{ij}\bar{\chi}_iSN_{R,j} + \text{h.c..} \qquad (2.9)
$$

Since S is real, this interaction breaks χ-number, but there is still a $\mathbb{Z}_2$ under which S, ϕ and all three χ are odd. This interaction makes it possible for out-of-equilibrium decays of the right-handed neutrino to generate a χ asymmetry through interference between tree-level and one-loop contributions with CP violating phases, in the exact same way that the same decays also generate a lepton asymmetry. The couplings in $\mathcal{L}_{\text{fermion}}$ which are assumed to be of order one will lead to efficient annihilation of the symmetric component of χ. Note that there is no hierarchy problem associated with the scalar S, because it need not be light. The only requirement for this mechanism to work is for S to not be heavier than the near-GUT scale right-handed neutrinos. Below the mass of S, χ-number becomes an accidental symmetry. Both due to the presence of this symmetry, and due to the fact that both ϕ and χ are singlets under the weak $SU(2)$, the dark sector does not participate in the sphaleron processes which allow the original asymmetry in the SM lepton sector to be transferred to the baryons.

Note that while the same mechanism generates the lepton and χ asymmetries, the phases that determine the size of the generated asymmetry are different. In particular, the lepton asymmetry will depend on the physical combinations of phases in the matrices y_{ij}^L and y_{ij}^N, whereas the χ asymmetry will depend on the phases in the matrices λ_{ij} and y_{ij}^S. This means that if the phases that are relevant for the χ asymmetry are smaller than those that are relevant for the lepton asymmetry, the χ asymmetry will be smaller, and therefore m_χ must be chosen so that the χ energy density will be a factor of 5-6 larger than the baryon energy density. We will not assume any particular relation between the phases in the lepton and χ sectors, treating m_χ as a free parameter that is chosen such that χ has an energy density compatible with the DM density we observe in the universe today.

The collider phenomenology of asymmetric FDM is identical to the symmetric case, which was studied in Ref. [23], and we will not go into this in any further detail (See Sec. V for further comments). Any indirect detection signals for the symmetric case are of course nonexistent for the asymmetric case, so we will not have anything further to say about constraints from indirect detection either. In the rest of the chapter we will concentrate on direct detection searches, where asymmetric FDM can have very different prospects compared to the symmetric case, due to the presence of interference, as we will study in detail in the next section.

2.2   Direct Detection

In this section we will calculate the cross section for χ to scatter off of an atomic nucleus, keeping interference terms. As mentioned in the introduction, when the DM is symmetric, the interference terms will cancel once the scattering of both χ and $\bar{\chi}$ are taken into account, but for asymmetric DM, they will be crucial. Based on the model of section 2.1, it is easy to see that scattering can happen at tree-level through Higgs exchange. At tree-level, the FDM interaction of Eqs. (2.1) and (2.2) (for the scalar and fermion DM cases, respectively) does not contribute to the scattering, however as was studied in Ref. [23], it does give rise to vector exchange at loop order. The exchanged vector boson can be either the photon or the Z-boson, but of course the latter is strongly suppressed compared to the former due to the Z-mass. Therefore we will only consider the photon exchange for the rest of the chapter.

2.2.1 Scalar DM
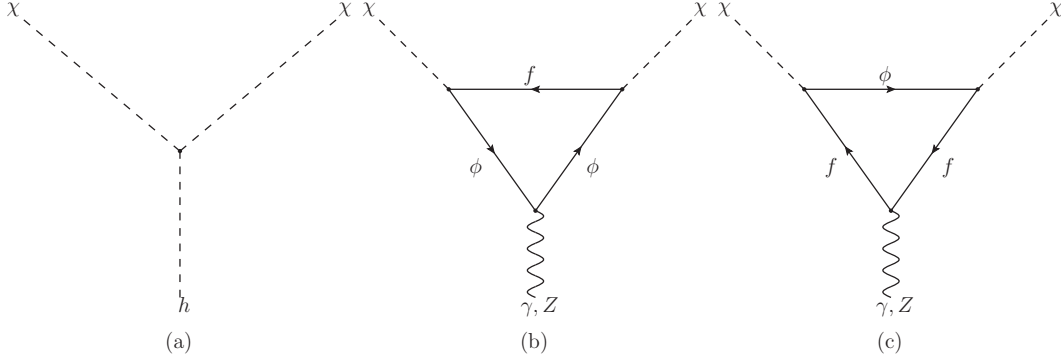
Figure 2.1: The Feynman diagrams that contribute to direct detection in the scalar DM case, namely tree level Higgs exchange (a) and γ/Z exchange with the vector boson line attached to either the mediator ϕ (b) or to the SM fermions f (c) running in the loop.

After electroweak symmetry breaking, the interaction term in Eq. (2.4) contains the interaction

$$\mathcal{L}_h \supset -v\lambda_{\chi h}\chi^*\chi h, \tag{2.10}$$

which leads to the tree-level Higgs exchange. The loop-induced coupling of the DM to the photon is calculated in Appendix A.3 and in the zero external momentum limit it has the form

$$b_\chi \partial^\mu \chi^* \partial^\nu \chi F_{\mu\nu}, \tag{2.11}$$

where

$$b_\chi \equiv -\frac{\lambda_\phi^2 e}{16\pi^2 m_\phi^2}\left(1 + \frac{2}{3}\ln\frac{m_\ell^2}{m_\phi^2}\right), \tag{2.12}$$

and m_ℓ is the mass of the tau lepton since we have assumed χ_τ to be the DM. The Feynman diagrams for these couplings are shown in figure 2.1.

Combining this with the Higgs and photon propagators, we can write the effective operators that give rise to the DM-nucleus scattering:

$$\mathcal{L}_{\text{eff}} = c_\gamma^q \chi^* \overset{\leftrightarrow}{\partial}^\mu \chi \bar{q}\gamma_\mu q + c_h^q \chi^* \chi \bar{q} q, \tag{2.13}$$

where the coefficients are related to the couplings in the UV theory as

$$c_\gamma^q = eQ_q \frac{b_\chi}{2}, \quad c_h^q = \frac{\lambda_{\chi h} m_q}{m_h^2}. \tag{2.14}$$

For the next step in calculating the scattering cross section, we convert from quark-level operators to effective nucleon-level operators and we take the nonrelativistic limit of the matrix elements, which gives $(N = p, n)$

$$\mathcal{L}_{\text{eff}} = c_\gamma^N \chi^* \overset{\leftrightarrow}{\partial}{}^\mu \chi \overline{N} \gamma_\mu N + c_h^N \chi^* \chi \overline{N} N. \tag{2.15}$$

The coefficients c^N at the nucleon level can be written in terms of the coefficients c^q at the quark level as

$$c_\gamma^N = \frac{e b_\chi}{2} \sum_q Q_q, \tag{2.16}$$

$$c_h^N = \sum_{q=u,d,s} c_h^q \frac{m_N}{m_q} f_{Tq}^{(N)} + \frac{2}{27} f_{TG}^{(N)} \sum_{q=c,b,t} c_h^q \frac{m_N}{m_q}, \tag{2.17}$$

where we use the numerical values of $f_{Tq}^{(N)}$ and $f_{TG}^{(N)}$ given in Ref. [42]. Combining with Eq. (2.14) we arrive at

$$c_\gamma^N = \frac{e Q_N b_\chi}{2}, \tag{2.18}$$

$$c_h^N = \frac{\lambda_{\chi h} m_N}{m_h^2} \left(\frac{2}{9} + \frac{7}{9} \sum_{q=u,d,s} f_{Tq}^{(N)} \right). \tag{2.19}$$

The leading (spin-independent) contribution to the nucleon matrix elements of the operators of Eq. (2.15) are

$$\langle \chi, N \left| \chi^* \overset{\leftrightarrow}{\partial}{}^\mu \chi \overline{N} \gamma_\mu N \right| \chi, N \rangle = 4 m_\chi m_N,$$

$$\langle \chi, N \left| \chi^* \chi \overline{N} N \right| \chi, N \rangle = 2 m_N. \tag{2.20}$$

Putting everything together, we define the dark matter-nucleon effective couplings

$$\mathcal{C}^N = 4 m_\chi m_N c_\gamma^N + 2 m_N c_h^N, \tag{2.21}$$

in terms of which the total scattering cross section is given by

$$\sigma_T = \frac{1}{16\pi} \left(\frac{1}{m_\chi + m_p} \right)^2 [Z\mathcal{C}^p + (A - Z)\mathcal{C}^n]^2. \tag{2.22}$$

15
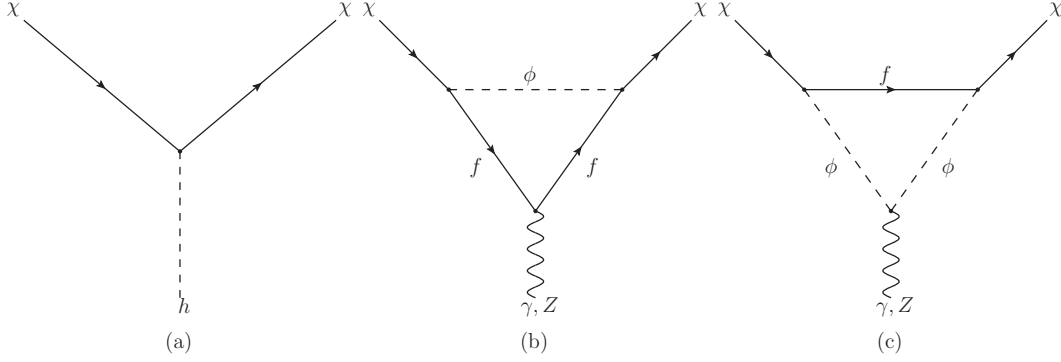
Figure 2.2: The Feynman diagrams that contribute to direct detection in the fermion DM case, namely tree level Higgs exchange (a) and γ/Z exchange with the vector boson line attached to either the mediator ϕ (b) or to the SM fermions f (c) running in the loop

2.2.2 Fermion DM

The calculation of the scattering cross section for the fermion DM case proceeds through the same steps as in the scalar DM case. The tree-level Higgs exchange arises from the interaction of Eq. (2.6) after electroweak symmetry breaking

$$\mathcal{L}_h \supset -\lambda_{\chi h}\bar{\chi}\chi h, \tag{2.23}$$

while the loop induced coupling of the DM to the photon is given by

$$\mathcal{L}_{\text{eff}} = b_\chi \bar{\chi}\gamma_\nu\chi\partial_\mu F^{\mu\nu} + \mu_\chi\bar{\chi}i\sigma_{\mu\nu}\chi F^{\mu\nu}, \tag{2.24}$$

where b_χ and the magnetic dipole moment μ_χ are defined as

$$b_\chi = -\frac{\lambda_\phi^2 e}{64\pi^2 m_\phi^2}\left(1 + \frac{2}{3}\log\frac{m_\ell^2}{m_\phi^2}\right), \tag{2.25}$$

$$\mu_\chi = -\frac{\lambda_\phi^2 e m_\chi}{64\pi^2 m_\phi^2}. \tag{2.26}$$

Note that this agrees with Ref. [23]. The Feynman diagrams for these couplings are shown in figure 2.2. The relativistic effective Lagrangian describing the interaction of the DM with quarks is

$$\mathcal{L}_{\text{eff}} = c_h^q\bar{\chi}\chi\bar{q}q + c_\gamma^q\bar{\chi}\gamma^\mu\chi\bar{q}\gamma_\mu q + c_{\text{md}}^q\bar{\chi}i\sigma^{\alpha\mu}\frac{k_\alpha}{k^2}\chi\bar{q}\gamma_\mu q, \tag{2.27}$$

16

where

$$c_h^q = \frac{\lambda_{\chi h} m_q}{v m_h^2}, \quad c_\gamma^q = e Q_q b_\chi, \quad c_{\text{md}}^q = e Q_q \mu_\chi. \tag{2.28}$$

We next convert the quark-level operators to nucleon-level operators and take the nonrelativistic limit. Details of the matching of operator coefficients between the quark and nucleon level operators can be found in Appendix A.5. We thus arrive at the effective Lagrangian at the nucleon level $(N = p, n)$

$$
\begin{aligned}
\mathcal{L}_{\text{eff}} &= c_h^N \overline{\chi}\chi \overline{N}N + c_\gamma^N \overline{\chi}\gamma^\mu\chi \overline{N}\gamma_\mu N \\
&\quad + c_Q^N \overline{\chi} i\sigma^{\alpha\mu} \frac{k_\alpha}{k^2} \chi \overline{N} K_\mu N \\
&\quad + c_\mu^N \overline{\chi} i\sigma^{\alpha\mu} \frac{k_\alpha}{k^2} \chi \overline{N} i\sigma^{\beta\mu} k_\beta N.
\end{aligned}
\tag{2.29}
$$

Here K_μ is the sum of the incoming and outgoing nucleon momenta, and the coefficients c^N are related to the c^q as

$$c_h^N = \sum_{q=u,d,s} c_h^q \frac{m_N}{m_q} f_{Tq}^{(N)} + \frac{2}{27} f_{TG}^{(N)} \sum_{q=c,b,t} c_h^q \frac{m_N}{m_q}, \tag{2.30}$$

$$c_\gamma^N = e b_\chi \sum_q Q_q, \tag{2.31}$$

and the charge and magnetic coefficients of the magnetic dipole moment are

$$c_Q^N = e Q_N \mu_\chi / 2 m_N, \quad c_\mu^N = -e \tilde{\mu}_N \mu_\chi / 2 m_N, \tag{2.32}$$

where $\tilde{\mu}_N$ is the nucleon magnetic moment, with $\tilde{\mu}_p = 2.8$ and $\tilde{\mu}_n = -1.9$.

So far we have kept the magnetic dipole terms. Their momentum dependence makes it impossible to write the differential event rate as the product of the elastic cross section and the velocity integration. We calculate the differential rate numerically, and work out the exclusion limits from LUX [43] in the presence of the dipole terms in Appendix A.5. The result is shown in Fig. 2.3. We find that the effect of the magnetic dipole operator is negligible compared to the charge operator in setting limits for the coupling λ_ϕ. Based on this, for the rest of the chapter we will drop the magnetic dipole contributions.

The leading (spin-independent) contribution to the nucleon matrix elements are

$$
\begin{aligned}
\langle \chi, N \left| \overline{\chi}\gamma^\mu\chi \overline{N}\gamma_\mu N \right| \chi, N \rangle &= 4 m_\chi m_N, \\
\langle \chi, N \left| \overline{\chi}\chi \overline{N}N \right| \chi, N \rangle &= 4 m_\chi m_N.
\end{aligned}
\tag{2.33}
$$
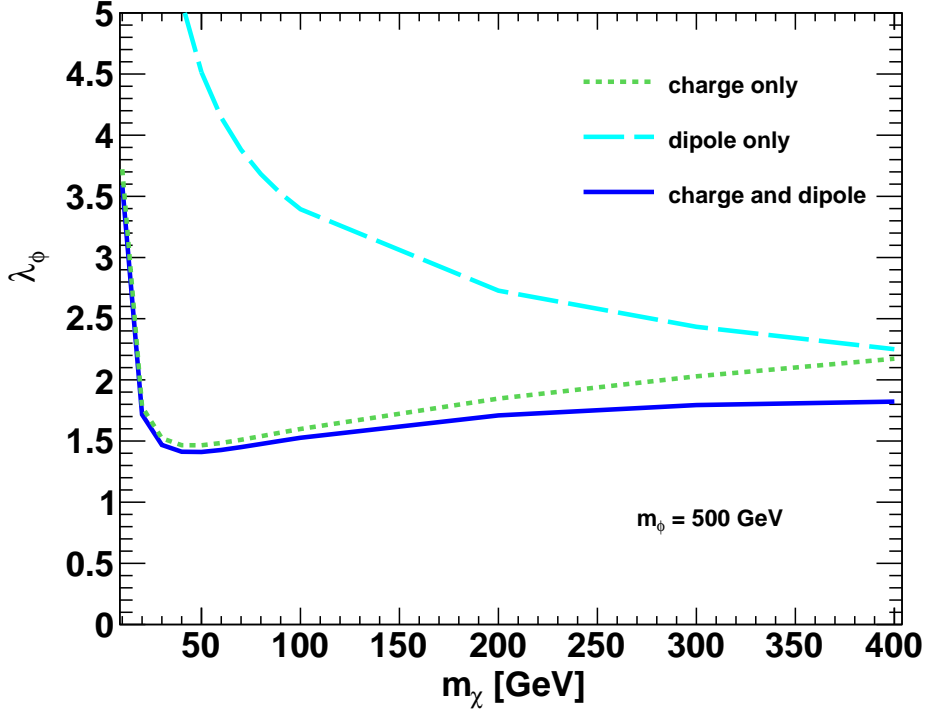
Figure 2.3: The LUX bound on the coupling λ_ϕ for $m_\phi = 500$ GeV calculated using the charge term alone, the dipole term alone, and the full combination.

As in the scalar DM case, we define the dark matter-nucleon effective couplings

$$\mathcal{C}^N = 4m_\chi m_N c_\gamma^N + 4m_\chi m_N c_h^N, \tag{2.34}$$

where the coefficients are

$$c_\gamma^N = -Q_N \frac{\lambda_\phi^2 e^2}{64\pi^2 m_\phi^2} \left(1 + \frac{2}{3}\log\frac{m_\ell^2}{m_\phi^2}\right), \tag{2.35}$$

$$c_h^N = \frac{\lambda_{\chi h} m_N}{v m_h^2}\left(\frac{2}{9} + \frac{7}{9}\sum_{q=u,\,d,\,s} f_{Tq}^{(N)}\right). \tag{2.36}$$

The total scattering cross section is then given by

$$\sigma_T = \frac{1}{16\pi}\left(\frac{1}{m_\chi + m_p}\right)^2 [Z\mathcal{C}^p + (A-Z)\mathcal{C}^n]^2. \tag{2.37}$$

18

2.3 Results

In this section, we use the cross section formulas derived in the Sec. 2.2 in order to calculate the bounds on lepton-flavored DM and directly compare the regions of parameter space that have been excluded for the symmetric and asymmetric cases. Note that the full parameter space of our model is four-dimensional (with the two masses m_χ, m_ϕ and the two couplings λ_ϕ and $\lambda_{\chi h}$) and therefore it is not possible to visually represent the phenomenological aspects of a full parameter scan. Instead, we choose to present the highlights in two pairs of complementary plots (for the scalar DM and fermion DM cases each), one pair where the masses are fixed at representative values and the couplings are varied, and one pair where the masses are varied, and a particular value of the couplings is chosen for each mass point. Combining the information in these plots, the reader should be able to develop an intuitive understanding for the prospects of the model in the full parameter space.

For the asymmetric scalar and fermion DM cases, we show in Fig. 2.4 and in Fig. 2.5 (respectively) the regions in the $(\lambda_{\chi h}, \lambda_\phi)$ plane for some representative choices of m_χ and m_ϕ that are consistent with the bounds from LUX [43]. We also check the bounds from CREEST, CDMS-Si, and SuperCDMS [44, 45, 46], but we find that the LUX bound dominates as long as $m_\chi \gtrsim 5$ GeV. Such low values of m_χ are not very interesting however, as $\lambda_{\chi h}$ has to be very small in order to be consistent with the invisible Higgs decay bounds [47, 48], namely $\mathrm{BR}_{h \to \bar{\chi}\chi} < 0.58$. We only plot $\lambda_\phi > 0$ since the cross section depends only on λ_ϕ^2, whereas the sign of $\lambda_{\chi h}$ is physical. We restrict ourselves to $|\lambda_{\chi h}| < 0.25$ in the fermion DM case, since the χ-Higgs coupling in this case arises from a higher-dimensional operator which is generated at $\Lambda \gtrsim$ TeV [see Eq. (2.7)]. Note that the allowed parameter regions lie in a band around a curve of maximal interference. The curve of maximal interference is a parabola since the Higgs exchange amplitude scales as $\lambda_{\chi h}$ while the photon exchange amplitude scales as λ_ϕ^2. In fact, the effective DM-photon coupling scales as λ_ϕ^2/m_ϕ^2, which explains why in the right plots the parabola moves toward the vertical axis with increasing m_ϕ. While many features are similar for the scalar and fermion DM cases, one difference stands out: as can be seen the left plots, for scalar DM both the shape of the curve of maximal interference as well as the size of the allowed region around this curve depend sensitively on m_χ while for fermion DM the allowed region is much less sensitive to m_χ. This is due to the difference between Eqs (2.20) and (2.33), where in

19
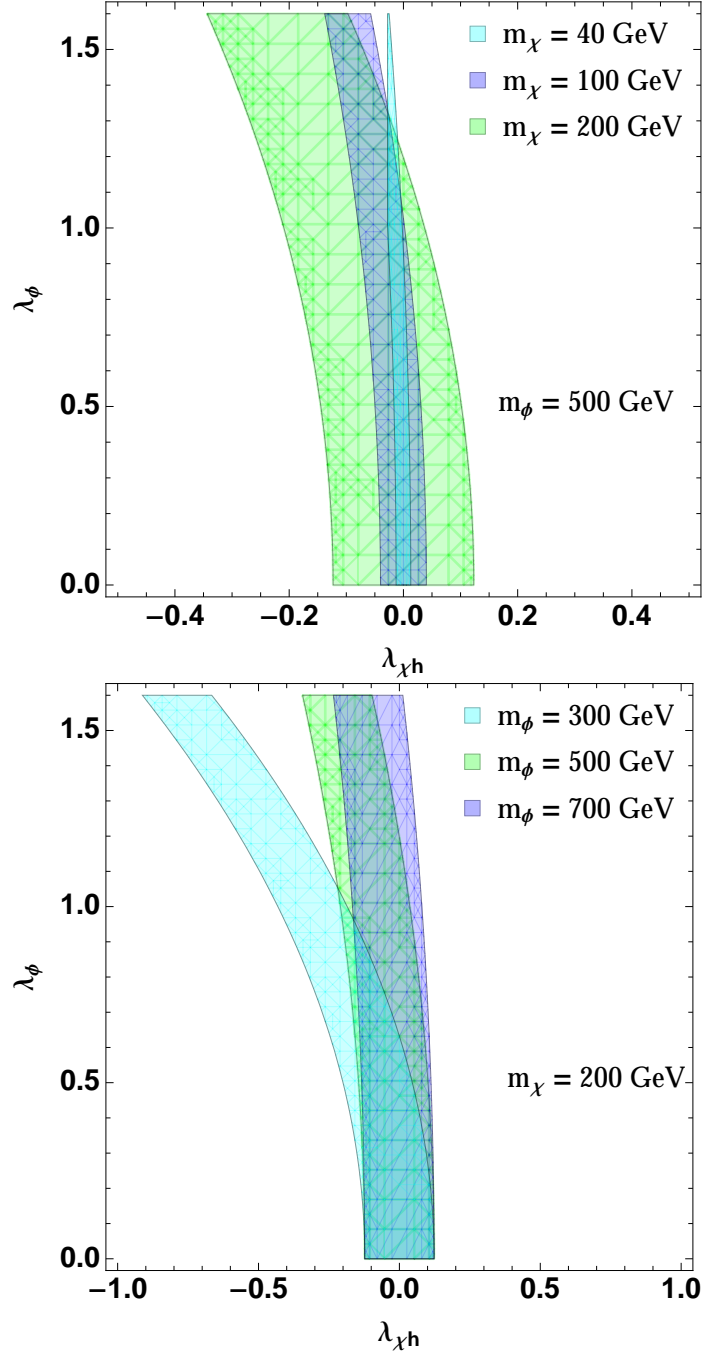
Figure 2.4: The region in the $(\lambda_{\chi h}, \lambda_\phi)$ plane for the asymmetric scalar DM case consistent with the LUX bound. (Left) m_ϕ fixed at 500 GeV while m_χ is varied. (Right) m_χ is fixed at 200 GeV while m_ϕ is varied. For $m_\chi = 40$ GeV, the allowed region is limited to small values of $\lambda_{\chi h}$ because of the invisible Higgs decay bound.
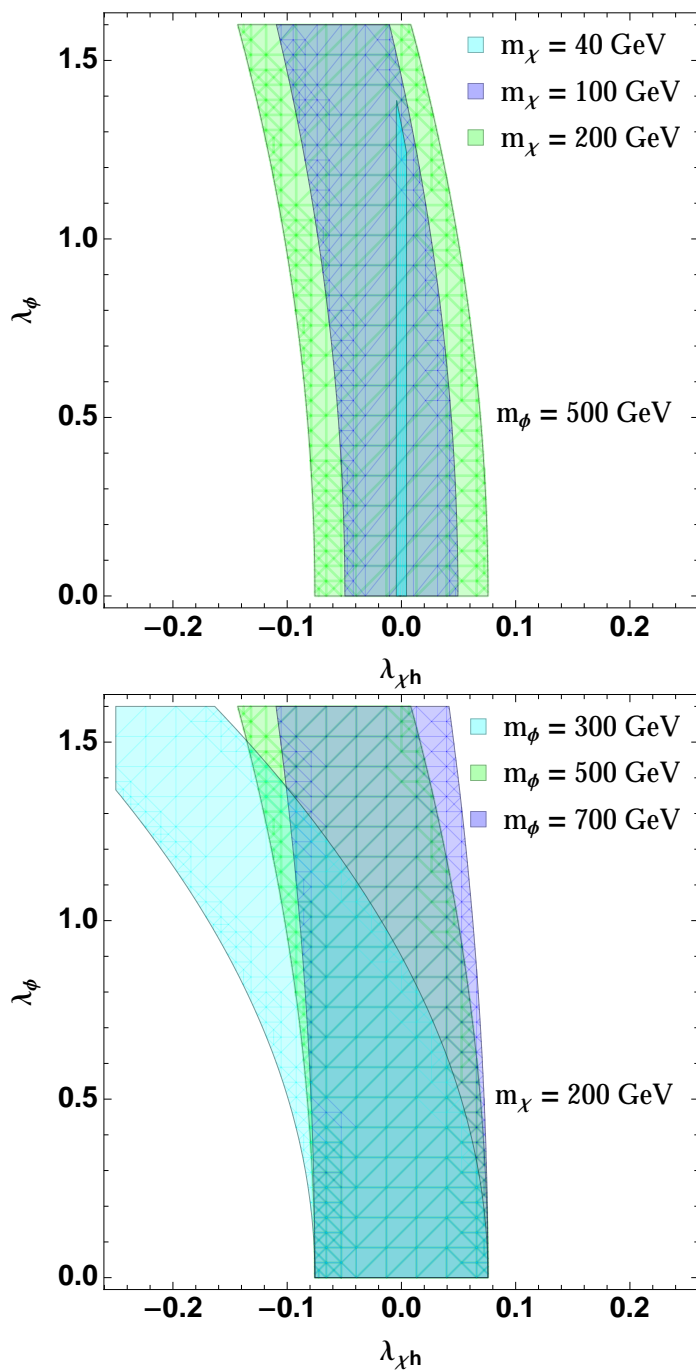
Figure 2.5: The region in the $(\lambda_{\chi h}, \lambda_\phi)$ plane for the asymmetric fermion DM case consistent with the LUX bound. (Left) m_ϕ fixed at 500 GeV while m_χ is varied. (Right) m_χ is fixed at 200 GeV while m_ϕ is varied. For $m_\chi = 40$ GeV, the allowed region is limited to small values of $\lambda_{\chi h}$ because of the invisible Higgs decay bound.

the scalar DM case the scaling of the Higgs-exchange and photon-exchange nuclear matrix elements with m_χ is different, while the scaling is the same in the fermion DM case.

Next, we contrast the regions in the parameter space that can be consistent with the LUX bound for symmetric and antisymmetric lepton-flavored DM as a function of the masses m_χ and m_ϕ. In the left plot of Figs. 2.6 and 2.7 (for scalar and fermion DM, respectively), we start by calculating for any point in the m_χ-m_ϕ plane the value of λ_ϕ that gives rise to the correct relic density in the symmetric DM case (for details of the relic abundance calculation, see Appendix A). For the symmetric DM case, we then check whether this parameter point is excluded by direct detection, keeping $\lambda_{\chi h} = 0$, since for the symmetric case the two channels add incoherently so any finite value of $\lambda_{\chi h}$ only strengthens the direct detection constraint. Next, for the same value of λ_ϕ, we check whether there is any value of $\lambda_{\chi h}$ (within the interval [-1.5, 1.5] for scalar DM and [-0.5, 0.5] for fermion DM, and consistent with the invisible Higgs decay bound if $2m_\chi < m_h$) for which asymmetric DM can be consistent with the direct detection bound. In the second plot (right), we exchange the roles of $\lambda_{\chi h}$ and λ_ϕ and repeat the same procedure, in other words $\lambda_{\chi h}$ is now fixed at the value which gives the correct relic abundance for the symmetric DM (both signs are considered) at any value of m_χ and m_ϕ (subject to the same constraints as mentioned above), and for antisymmetric DM λ_ϕ is allowed to float in looking for consistency with the direct detection bound. Note that we have excluded the regions $m_\phi < 105$ GeV in these plots due to ϕ-pair production bounds from LEP. This is only meant as a conservative approximation to the LEP bound, however the direct search bounds from the LHC (such as stau searches) will rule out this region in any case and extend further, and for this reason the lowest m_ϕ regions should not be taken too seriously. A full analysis of the LHC constraints will be studied in upcoming work, but it is outside the scope of this paper due to the large number of LHC searches that need to be recast. Since pair production cross sections of noncolored particles (especially scalars) fall off very rapidly however, we do not expect the inclusion of LHC bounds to drastically change plots 2.6 and 2.7.

While choosing either $\lambda_\phi = 0$ or $\lambda_{\chi h} = 0$ for the symmetric case in Figs. 2.6 and 2.7 may appear to be somewhat arbitrary, this in fact allows us to fully map out the exclusion region from direct detection bounds, in the following sense: If a point in the m_χ-m_ϕ plane is excluded by LUX in both Figs. 2.6 and 2.7 in the symmetric
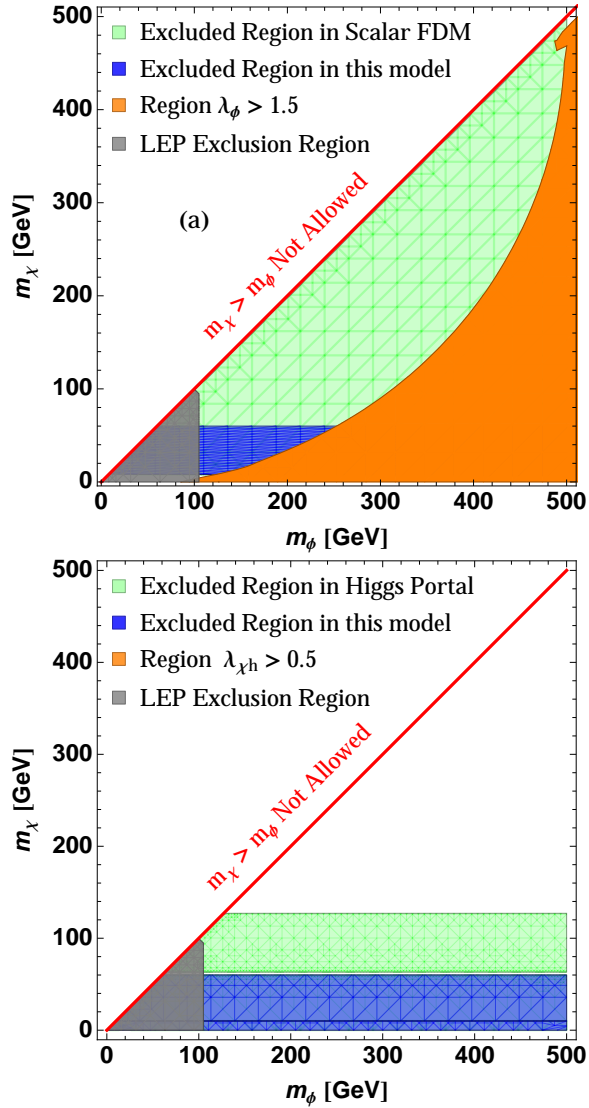
Figure 2.6: The excluded region in the m_χ-m_ϕ plane for scalar DM. For the left plot, λ_ϕ is calculated point by point to give the correct relic abundance for symmetric DM. The orange region includes points where this calculated value exceeds 1.5. The green region then shows the points excluded by direct detection for symmetric DM using this value of λ_ϕ. The blue region shows points where direct detection also excludes asymmetric DM for the same value of λ_ϕ, and for any value of $\lambda_{\chi h}$ (subject to $|\lambda_{\chi h}| < 1.5$; for $2m_\chi < m_h$, consistency with the invisible Higgs decay bound is also required). For the right plot, the roles of λ_ϕ and $\lambda_{\chi h}$ are reversed, and both signs of $\lambda_{\chi h}$ are used in plotting the blue region. See the main text for further details.
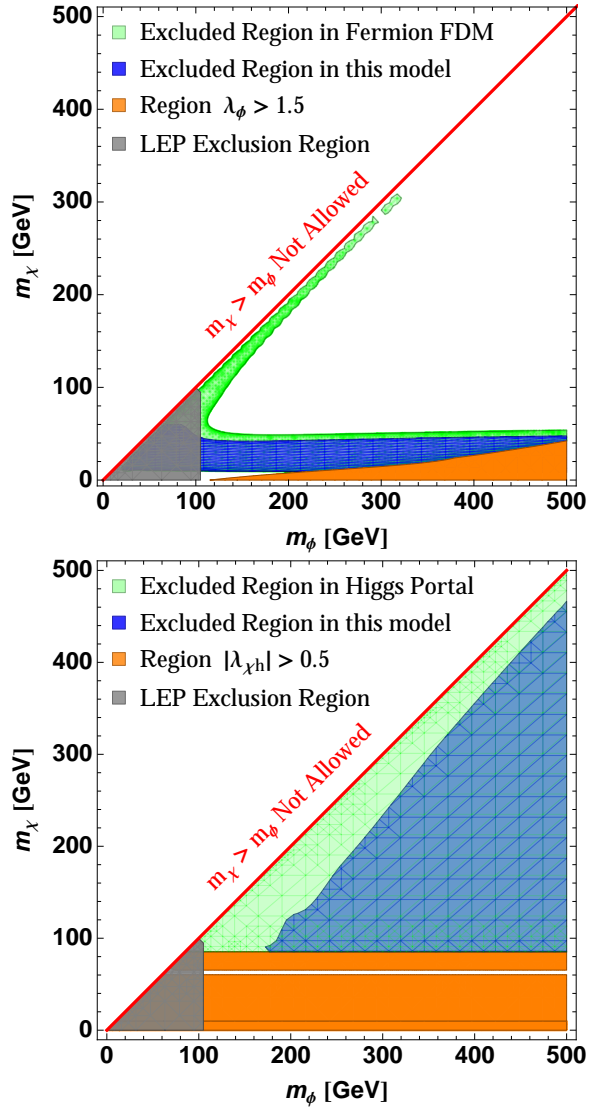
Figure 2.7: The excluded region in the m_χ-m_ϕ plane for fermion DM. For the left plot, λ_ϕ is calculated point by point to give the correct relic abundance for symmetric DM. The orange region includes points where this calculated value exceeds 1.5. The green region then shows the points excluded by direct detection for symmetric DM using this value of λ_ϕ. The blue region shows points where direct detection also excludes asymmetric DM for the same value of λ_ϕ, and for any value of $|\lambda_{\chi h}| < 0.5$ (for $2m_\chi < m_h$, consistency with the invisible Higgs decay bound is also required). For the right plot, the roles of λ_ϕ and $\lambda_{\chi h}$ are reversed, and both signs of $\lambda_{\chi h}$ are used in plotting the blue region. See the main text for further details.

case, it is ruled out even when both couplings are allowed to vary, subject to the relic abundance constraint, as we will now argue. Interference is absent in the symmetric case in calculating the scattering rate for direct detection, which therefore can be written as $C_{DD,\phi}(\lambda_\phi^2)^2 + C_{DD,h}\lambda_{\chi h}^2$ for some constants $C_{DD,\phi}$ and $C_{DD,h}$. Similarly, the cross section of DM annihilation relevant for the relic abundance calculation can also be written as $C_{RA,\phi}(\lambda_\phi^2)^2 + C_{RA,h}\lambda_{\chi h}^2$, for the same reason[3]. Thus, for a given mass point, obtaining the correct relic abundance constrains the model to lie on an ellipse in the λ_ϕ^2-$\lambda_{\chi h}$ plane, with the major axis pointing along either the λ_ϕ^2 or the $\lambda_{\chi h}$ axis. Moreover, the contours corresponding to constant scattering rate in a direct detection experiment are also ellipses with their major axis pointed along either the λ_ϕ^2 or the $\lambda_{\chi h}$ axis. Thus, as one moves around the ellipse for obtaining the correct relic abundance, one will always find the point with the smallest direct detection scattering rate where the family of ellipses from direct detection are tangent to the ellipse from relic abundance. Since both ellipses are pointed along one of the coordinate axes, this will happen on one of the coordinate axes, thus there can be no point with both couplings nonzero that can result in a smaller scattering rate for direct detection than at the points with one of the couplings equal to zero.

There are many interesting features in Figs. 2.6 and 2.7, which we now go over in detail. First of all, note that for symmetric DM, the entire parameter region is excluded for fermion DM with negligible FDM coupling (right plot in Fig. 2.7, apart from a very narrow band near the Higgs resonance region, where $\lambda_{\chi h}$ can be very small). This exclusion extends all the way down to zero mass due to the invisible Higgs bound. Similarly, scalar DM with negligible Higgs coupling (left plot in Fig. 2.6) is also ruled out for a DM mass above 8 GeV, below which direct detection experiments lose sensitivity. The nearly-complete exclusion for these two cases is due to relic abundance requiring a very large coupling due to suppressions in the amplitude. Scalar DM with FDM interactions annihilates to leptons, so the s-wave annihilation is chirally suppressed [see Eq. A.5)] and therefore p-wave annihilation dominates. Fermion DM that annihilates through Higgs exchange is also velocity suppressed. In both cases, turning on both couplings for asymmetric DM opens up regions of parameter space that can be consistent with all constraints. In particular, for scalar

---

[3]There is a caveat here that the reaction $\chi\chi \to \tau\tau$ does in fact have a cross term between ϕ and h exchange. However, the Yukawa coupling of the τ is small enough that this term can be neglected for all practical purposes.

DM, the only region that is ruled out is for $2m_\chi < m_h$ where the invisible Higgs decay bound forces $\lambda_{\chi h}$ to be very small such that the interference cannot be very effective. For fermion DM where we set $\lambda_{\chi h}$ by the relic abundance in the symmetric case (Fig. 2.7, right), the large m_ϕ region is ruled out even for the asymmetric case, because the effective DM-photon coupling scales as λ_ϕ^2/m_ϕ^2, so a value of λ_ϕ of order one is not strong enough to cancel the very large Higgs exchange contribution in direct detection.

There are also a few interesting features in the left plot of Fig. 2.7. For symmetric DM, the exclusion region extends both to large m_ϕ for light m_χ, as well as to relatively large m_χ when $m_\phi - m_\chi$ is small. The former region is ruled out because both direct detection and relic abundance depend on λ_ϕ and m_ϕ in the same way, thus the direct detection constraint does not weaken even at large m_ϕ. The latter region is ruled out because the loop that gives rise to the effective DM-photon coupling is enhanced in this kinematic regime, and therefore the direct detection bound is stronger than one would naively expect. In a way similar to Fig. 2.6 (left), the excluded region for asymmetric DM is basically due to the invisible Higgs decay bound, which forces $\lambda_{\chi h}$ to remain small, and therefore makes the interference ineffective. Also similar to Fig. 2.6 (left), the region $m_\chi < 10$ GeV is not excluded because direct detection experiments lose sensitivity at such low recoils.

2.4   Conclusion and Outlook

We have introduced the scenario of lepton-flavored asymmetric dark matter, where the same mechanism that generates a lepton asymmetry at high scales also generates a DM asymmetry, and we have studied the prospects of this scenario for direct detection experiments. In particular, we have emphasized the fact that the interactions present in the model lead to both Higgs and photon exchange in direct detection, and that the corresponding amplitudes are naturally of the right size such that interference can be important, leading to a significant weakening in the bounds reported by direct detection experiments. We have contrasted the regions of parameter space excluded by the null results of direct detection experiments for this scenario with the parameter space of the same model where no DM asymmetry is generated, and where therefore the interference effects cancel out once the scattering of both the DM particle and

its antiparticle off of nuclei are taken into account. In particular, we showed that in the symmetric case with fermion DM where the Higgs exchange dominates, the parameter space is entirely ruled out except for a narrow Higgs resonance window, while in the asymmetric case a large fraction of the parameter space is still allowed. The same conclusion also holds for scalar DM with a mass above 8 GeV when the FDM interaction dominates.

Turning to prospects of this model for future experiments, we note that the presence of interference in direct detection can be confirmed by separately determining the DM scattering rate off of protons and neutrons. This can be achieved in the next generation of direct detection experiments if more than one experiment with a nonidentical active detector material can observe a signal, since the ratios of protons to neutrons in the nuclei of the active materials will then be different. A separate measurement of the scattering rates from protons and neutrons can then be used to solve for λ_ϕ and $\lambda_{\chi h}$.

While indirect detection signals are absent for asymmetric DM, the collider phenomenology of our model is identical to the symmetric case. The discovery prospects in the multilepton final state at the LHC were studied in Ref. [23] at which point no collider constraints were available. It would now be interesting to study the constraints imposed on the lepton-flavored dark matter model by translating the searches performed by ATLAS and CMS in the dilepton and multilepton final states with and without transverse missing energy. Due to the multiplicity of such analyses this was outside the scope of this work, but these constraints will be studied in upcoming work.

In this chapter we considered it sufficient to simply outline the details of a model which would lead to the generation of a DM asymmetry during high-scale leptogenesis, and to remark that an order one coupling for the FDM interaction would then efficiently annihilate the symmetric part of the DM particles. In the following chapter we take up this question in greater quantitative detail and calculate the energy density left over in the asymmetric DM as a function of the parameters of a particular UV model.

Chapter Three: Secretly asymmetric dark matter[1]

Asymmetric dark matter (ADM) [31, 55, 33, 56, 32, 34, 37, 36] is motivated by the observation that the dark matter and baryon energy densities today are comparable, so that for dark matter masses of a few GeV, the number densities of the dark and visible sectors are also roughly comparable. The baryon number density today is set by an asymmetry, which suggests that dark matter could also be asymmetric, with the origin of the two asymmetries being related. In order to realize the conventional ADM scenario, a mechanism has to be put in place in order to break $U(1)_\chi$, a symmetry which guarantees conservation of dark matter (DM) number, in much the same way that baryon number has to be broken in order to generate an asymmetry in the visible sector.

In this chapter we study the possibility that for a dark sector with multiple states, the ADM paradigm can be realized without having to break $U(1)_\chi$. Asymmetries can be generated in the different dark sector states, while keeping the total charge under the $U(1)_\chi$ at zero. If heavier states in the dark sector decay to lighter ones after DM annihilations have frozen out [35, 57], then the final DM population is in fact symmetric, even though its abundance was set by an asymmetry. For this reason we will refer to this mechanism as Secretly Asymmetric Dark Matter (SADM). The idea of repopulating the symmetric component of DM at late times through oscillations has also been explored [58, 59, 60, 61, 62].

The relic abundance of DM in this mechanism is in some ways similar to the abundance of charged stable particles in the Standard Model (SM). Even though the abundances of baryons and leptons are set by an initial asymmetry, the universe is always charge neutral and $U(1)_{\mathrm{EM}}$ is never broken. If protons were to decay at late times, the universe could end up with a symmetric population of electrons and positrons which is secretly asymmetric.

---

[1]This chapter is based on work previously published as ref. [54]. This author contributed to the methodology, calculations, and text of this paper.

3.1 The Generation of the Asymmetry

Flavored dark matter (FDM) models [63, 21, 23, 64, 24, 65, 27, 29, 28, 4, 66, 67, 68, 69, 70, 71, 72] have multiple dark matter states by construction, as well as a simple way to connect the DM states with baryons or leptons that allows the transfer of asymmetries between the two sectors. Therefore, the SADM mechanism can be naturally realized in FDM models. In this work we will use a model of lepton flavored dark matter to demonstrate how the proposed mechanism works. We will assume that high-scale leptogenesis [38] (see refs. [73, 74] for a review and comprehensive list of references) generates an asymmetry in the lepton sector, which will then be transferred to baryons and to the dark sector.

Specifically, consider a model of FDM in which three flavors of SM singlet Dirac fermions $(\chi, \chi^c)_i$ $(i = 1, 2, 3)$ interact with the right-handed leptons of the SM via a scalar mediator ϕ, with the interaction given by

$$\mathcal{L}_{\text{FDM}} = \lambda_{ij} \, \phi \, \chi_i \, e_j^c + \text{h.c.} \tag{3.1}$$

We will denote the mass of the lightest χ by m_χ and the typical mass splitting between the χ flavors by δm.

It is worth commenting on the conserved quantum numbers in the presence of the interaction in equation 3.1. Individual lepton numbers L_i in the SM can be extended by assigning charges to χ_i. We will refer to the extended lepton numbers by $\tilde{L}_i$. Then $U(1)_{B-\tilde{L}}$ remains unbroken and anomaly-free, except for the explicit breaking from heavy right-handed neutrinos. If the coupling matrix λ_{ij} is flavor-diagonal in the charged lepton and χ mass basis, the $U(1)_{\tilde{L}}^3$ flavor symmetry is preserved to a good approximation at low energies, broken only by the light neutrino mass matrix. The neutrino masses are small enough to have no effect on the physics to be discussed here, and will therefore be neglected from here on. The presence of off-diagonal entries in the couplings λ_{ij} do have interesting phenomenological consequences; however for the sake of simplicity we will defer the discussion of these effects to a more detailed study and we will restrict ourselves to the flavor-universal case with $\lambda_{ij} \equiv \delta_{ij} \lambda$. Note that there is also a separate $U(1)_\chi$ symmetry under which all three χ_i have the same charge and the mediator ϕ has the opposite charge.

As mentioned above, we assume that out-of-equilibrium decays of the lightest right handed neutrino N_1 generate a net $B - \tilde{L}$ asymmetry in the SM sector. The
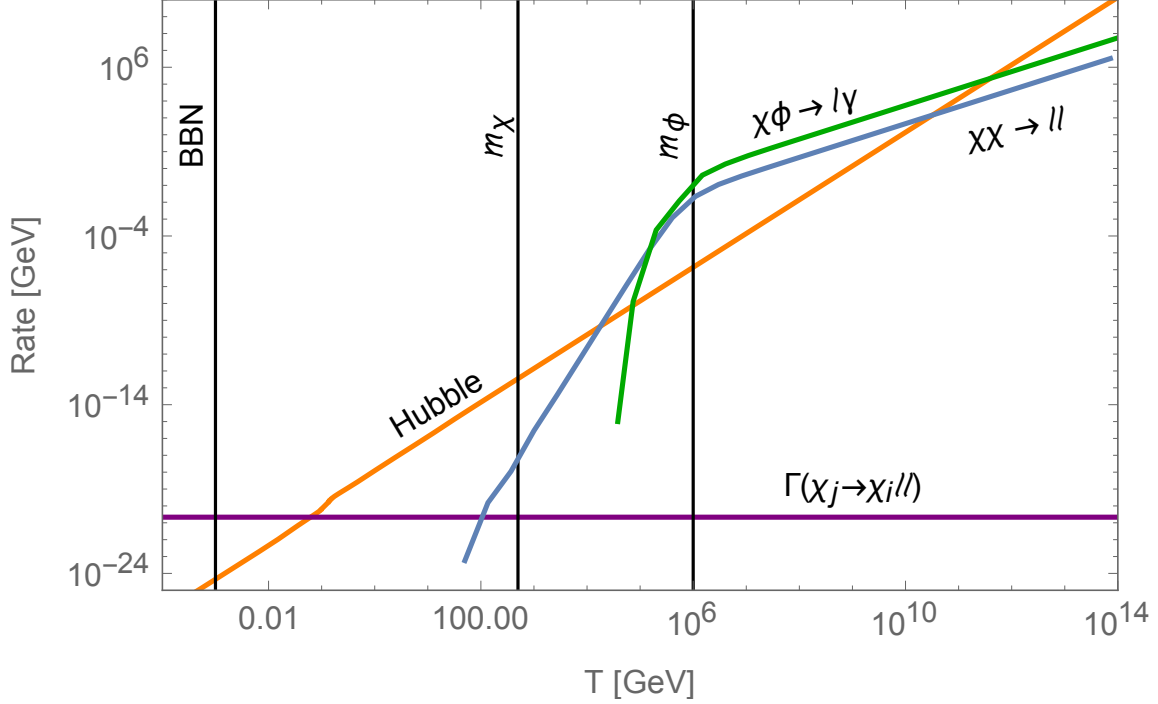
Figure 3.1: Rates of the most important FDM processes and the Hubble scale as a function of temperature for the parameter point defined in the main text.

comoving quantum numbers

$$\tilde{\Delta}_i = \left(B/3 - \tilde{L}_i\right)/s \equiv \Delta_i - \Delta Y_{\chi_i} \tag{3.2}$$

are conserved from the end of leptogenesis down to scales where neutrino oscillations become important. Here s is the entropy density, $Y_{\chi_i} = n_{\chi_i}/s$ are the comoving number densities of dark matter, and $\Delta_i = (B/3 - L_i)/s$ are the conserved comoving quantum numbers in the absence of the dark sector. Depending on which linear superposition of the e, μ and τ flavors N_1 couples to, leptogenesis generates nonzero values for these conserved quantities, which we will take as the initial conditions for the SADM mechanism.

Let us now follow the thermal history of the universe from the end of leptogenesis to lower temperatures. For concreteness we will use a specific parameter point ($\lambda = 0.05, m_\chi = 500$ GeV, $m_\phi = 10^6$ GeV, $\delta m = 0.4 m_\chi$, $T_{\text{leptogenesis}} > 10^{12}$ GeV), and in figure 3.1 we show for this parameter point how the rates of the most important processes in the model compare to the Hubble scale as a function of temperature.

With these values, the FDM interaction of equation 3.1 goes into chemical equilibrium after all N have decayed. This is not a necessary condition for the SADM mechanism to work and merely simplifies the discussion, as it lets us take initial conditions from leptogenesis (values of Δ_i, denoted henceforth as Δ_i^0) in a modular fashion. If the FDM interaction is already in equilibrium during leptogenesis one can solve the Boltzmann equation to track the asymmetries in the two sectors as a function of time.

As the universe continues to cool down, the asymmetry originally generated in the left-handed leptons is transferred to the right-handed leptons (through the SM Yukawas), the baryons (through sphalerons) and to the χ_i (through the FDM interactions). With all these interactions in equilibrium, the comoving asymmetries of all species can be related to the conserved quantities during this epoch (the $\tilde{\Delta}_i$) through equilibrium thermodynamics, with the constraints that the total hypercharge and the total $U(1)_\chi$ number of the universe stay zero. Since individual χ numbers are all zero until the FDM interaction goes into equilibrium, the value of $\left(\tilde{\Delta}_i\right)$ just after equilibrium is equal to the value of $(\Delta_i) - (\Delta Y_{\chi i})$ just before, namely Δ_i^0.

At our parameter point, the next step in the thermal evolution is the FDM interaction falling out of equilibrium as the temperature drops below m_ϕ. This decouples the SM and FDM sector asymmetries. Now the comoving asymmetries ΔY_{χ_i} are all separately conserved, and their values are given in terms of the initial conditions as

$$
\begin{pmatrix} \Delta Y_{\chi e} \\ \Delta Y_{\chi \mu} \\ \Delta Y_{\chi \tau} \end{pmatrix} = \frac{2}{15} \begin{pmatrix} -2 & 1 & 1 \\ 1 & -2 & 1 \\ 1 & 1 & -2 \end{pmatrix} \begin{pmatrix} \Delta_e^0 \\ \Delta_\mu^0 \\ \Delta_\tau^0 \end{pmatrix}.
\tag{3.3}
$$

At the same time, the total $B - \tilde{L}$ comoving asymmetry in the SM sector at early times can be related to the baryon number density B_0 and entropy density s_0 today,

$$
\Delta Y_{B-\tilde{L}} = \sum_i \Delta_i^0 \approx \frac{79}{28} \frac{B_0}{s_0},
\tag{3.4}
$$

which imposes a constraint on the possible initial conditions. From this point on, the thermal evolution of the SM sector proceeds as usual.

After the symmetric component of DM annihilates away (through mechanisms discussed below), the DM relic abundance today is given by

$$
\rho_{DM} = m_\chi \, s_0 \left(|\Delta Y_{\chi e}| + |\Delta Y_{\chi \mu}| + |\Delta Y_{\chi \tau}| \right).
\tag{3.5}
$$
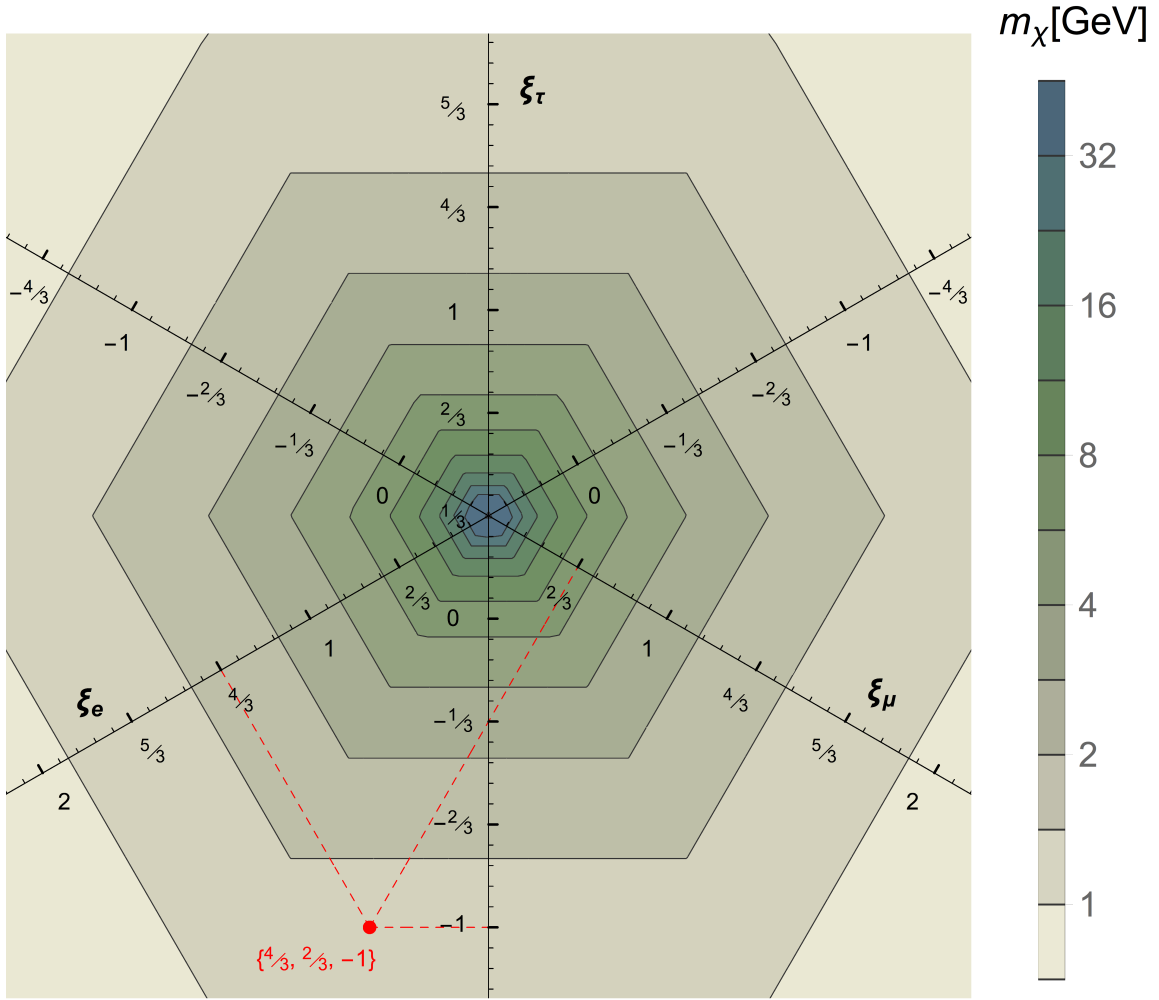
Figure 3.2: The values of m_χ needed to obtain the correct ρ_B and ρ_{DM} as the initial lepton asymmetries Δ_i^0 are varied subject to the constraint of equation 3.4, assuming there is no symmetric component to the relic. The values of $\xi_i \equiv \Delta_i^0 / \Delta Y_{B-L}$ for any point can be read off by drawing perpendiculars to the three axes shown.

Therefore, the ratio

$$\frac{\rho_B}{\rho_{DM}} = \frac{m_p}{m_\chi} \frac{28/79 \left(\Delta_e^0 + \Delta_\mu^0 + \Delta_\tau^0 \right)}{|\Delta Y_{\chi e}| + |\Delta Y_{\chi \mu}| + |\Delta Y_{\chi \tau}|} \tag{3.6}$$

relates the value of m_χ to observed values of ρ_B and ρ_{DM} (with $\rho_B/\rho_{DM} = 0.185$ [75]), given any initial condition Δ_i^0. This is illustrated in figure 3.2. Note that ρ_B and ρ_{DM} depend on different combinations of the initial conditions.

While for generic initial conditions we expect m_χ to be a few GeV, both larger and smaller values are possible in the following two limits: If the leptogenesis mechanism generates almost equal Δ_i^0 then equation 3.3 sets the ΔY_{χ_i} to be small, and therefore the DM mass needs to be large to obtain the right ρ_{DM}. On the other hand, if the leptogenesis mechanism generates large individual asymmetries for the SM lepton flavors that almost cancel [76] (e.g. $\Delta_\tau^0 = -\Delta_\mu^0 \gg \Delta_e^0 \sim \Delta Y_{B-L}$) then the denominator in equation 3.6 is large, and the DM mass needs to be small.

3.2   Decays in the dark sector

If the mass splitting $\delta m_{ij} \equiv m_{\chi_i} - m_{\chi_j}$ is less than $m_{\ell_i} + m_{\ell_j}$, the decays $\chi_i \rightarrow \chi_j + X$ can only proceed through χ-flavor mixing or through strongly suppressed loop processes [77], and the lifetime can be so long that all three χ can be treated as stable for practical purposes. For larger splittings however, the decay $\chi_i \rightarrow \chi_j \ell_i \bar{\ell}_j$ proceeds at tree level, with

$$\Gamma \simeq \frac{\lambda^4 (\delta m_{ij})^5}{480 \pi^3 m_\phi^4}. \tag{3.7}$$

If decays become important before χ-$\bar{\chi}$ annihilations freeze out, then they depopulate the heavier flavors and the dark matter abundance is set by the usual symmetric thermal freeze-out. Therefore, if the relic abundance based on the initial asymmetry is to survive at late times, then decays need to happen after annihilations freeze-out, but before Big-Bang Nucleosynthesis (BBN) in order to avoid early universe constraints. This is a core requirement of our set up. It is straightforward to check that this condition is satisfied at our parameter point. The width of the heavier flavors for these parameters is illustrated by the horizontal line in figure 3.1.

3.3 Annihilation of the symmetric DM component

If FDM annihilations $\chi_i \bar{\chi}_j \to l_i^- l_j^+$ are still active below $T \sim m_\chi$, then they deplete the asymmetry in the dark sector. Therefore, another core requirement for SADM is to ensure that the FDM interaction decouples while χ is relativistic. This also implies that we need additional interactions which can annihilate the symmetric component of DM, without depleting the asymmetry. We consider the setup, referred from here on as the Z'-model, where the $U(1)_\chi$ symmetry is gauged with a coupling g_D, and where the gauge boson Z'_μ acquires a small mass $m_{Z'} < m_\chi$. The Z' couples to the χ_i in a flavor-diagonal fashion and leads to efficient χ_i-$\bar{\chi}_i$ annihilations, such that the symmetric component of DM annihilates away for $g_D \gtrsim g_{\mathrm{WIMP}}$, where g_{WIMP} is the coupling that leads to the correct relic abundance for a thermal relic with the same mass.

Since ϕ carries a unit charge under $U(1)_\chi$ as well as hypercharge, it leads to kinetic mixing [78, 79] between these groups

$$\mathcal{L}_{\mathrm{mix.}} = -\frac{\epsilon}{2} B^{\mu\nu} Z'_{\mu\nu}, \tag{3.8}$$

where the loop of ϕ generates $\epsilon \sim 10^{-3} - 10^{-4}$ for couplings needed to annihilate the symmetric part. However, other UV contributions to the kinetic mixing can lead to a larger or smaller value of ϵ. The Z' can decay to the light SM fermions through the kinetic mixing.

3.4 Experimental Signatures of the Z'-model

If all flavors of χ are long-lived on cosmological timescales then there are no annihilations happening today and therefore indirect detection experiments are not sensitive to this case. If on the other hand only the lightest flavor survives today, then the DM distribution is symmetric. Since there is only a lower limit on g_D, one can obtain a stronger signal in indirect detection for a given m_χ compared to a WIMP. In particular, the annihilations will take the form $\bar{\chi}\chi \to Z'Z' \to 4f$, where f denotes SM fermions with $m_f < m_{Z'}/2$. Depending on $m_{Z'}$, the leading constraint from indirect detection may arise from positrons [80, 81], photons [82] or CMB measurements of
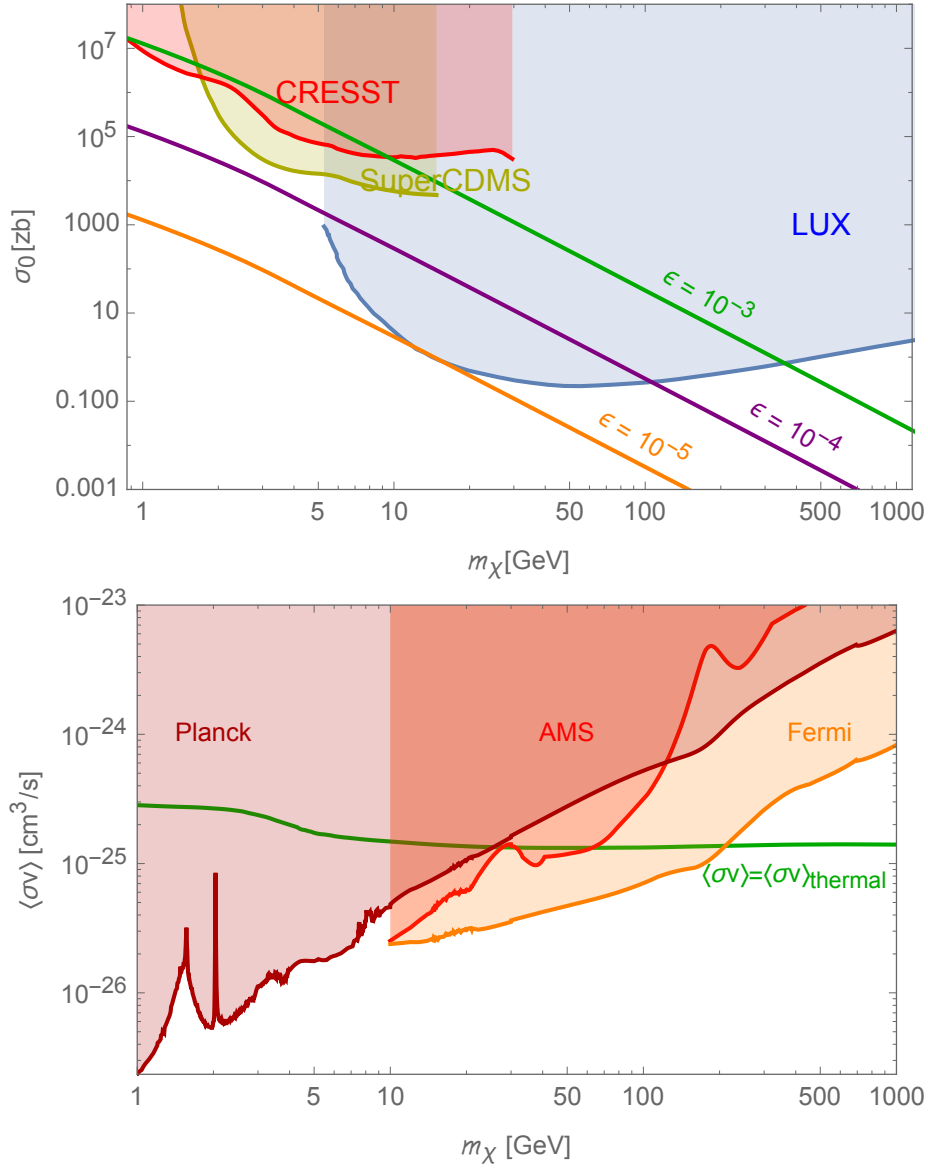
Figure 3.3:   Constraints on the Z'-model. *Left:* Direct detection constraints from LUX [86, 87], SuperCDMS [88] and CRESST-II [89] for representative values of ϵ and $g_D = g_{\text{WIMP}}$. *Right:* Indirect detection constraints from Planck [75], Fermi [82] and AMS [80, 81]. For reference we also show the annihilation cross section [90] which gives the correct relic abundance in our model with no asymmetry. $m_{Z'}$ is taken to be $m_\chi/2$ for both plots.

ionization [75]. These constraints were considered in ref. [83, 84, 85], and they are shown in the right-hand plot of figure 3.3.

The Z'-hypercharge mixing also gives rise to a signal in direct detection experiments such as LUX [86, 87], SuperCDMS [88] and CRESST-II [89]. Since tree-level Z-exchange is excluded by orders of magnitude, this translates to a strong constraint on the model parameters. In the left-hand plot of figure 3.3 we show the bounds in the m_χ-σ_0 plane for a specific choice of $m_{Z'} = m_\chi/2$.

Finally, there are also bounds on the model from dark photon searches, which can be quite stringent for a very light Z' [91, 92]. However for $m_{Z'} \gtrsim 1$ GeV, the bound for ϵ is typically at the 10^{-3} level, and generic values in our model are compatible with this constraint.

We see that direct detection, indirect detection and dark photon searches provide a complementary set of constraints for the parameter space of the Z' model. Light DM with $m_\chi \simeq 5$ GeV, which can be obtained from generic initial conditions (see figure 3.2), is unconstrained by direct detection even for generic values of ϵ, and can be within reach of future experiments probing light dark matter. The low m_χ region is in tension with indirect detection bounds, but the constraints may be evaded in a modified version of the model, for example if the main annihilation channel is into neutrinos. Heavier $m_\chi \gtrsim O(100$ GeV$)$ are unconstrained by either set of bounds.

3.5   Alternative model for annihilating the symmetric part

In order to stress the model dependence of some of the bounds considered above, we describe a variation of the model where DM annihilates via a scalar instead of a Z'. In particular, consider a light real scalar S with the interactions

$$\mathcal{L}_S = \kappa_{ij} S \chi_i \chi_j^c - V(S) \,. \tag{3.9}$$

Consistent with the $U(1)_L^3$ global symmetry we will take $\kappa_{ij} \equiv \delta_{ij}\kappa$. S develops a coupling to the right-handed SM leptons at one loop through the FDM interaction, and can therefore efficiently annihilate the symmetric part of the DM distribution. S does not mix with the Higgs boson until at least the two-loop order, and even this mixing is suppressed by lepton Yukawa couplings. Therefore, unlike the Z', tree-level S exchange only gives a negligible signal in direct detection experiments. Furthermore, the annihilation channel $\bar{\chi}\chi \to SS$ is p-wave suppressed, which means

that even for a fully symmetric χ distribution today, indirect detection signals are expected to be very weak. Thus, this alternative model is basically unconstrained by the experiments discussed above.

3.6 Conclusions

We have studied the SADM mechanism where for a dark sector with multiple states, the relic abundance is set by an asymmetry even though the DM number remains zero. If heavier DM states can decay to the lightest state, then DM is symmetric at late times, whereas otherwise multiple DM components can be present today. This mechanism is realized naturally in models of FDM. Experimental signals, if present, arise mainly due to the sector of the model that is responsible for annihilating the symmetric component of the DM. We have presented two alternatives for this sector: a Z'-model where Z'-hypercharge mixing generically takes place at the one-loop level, and a scalar model where mixing with the Higgs can naturally be very small. For the former model there are a number of experimental constraints from DM searches as well as dark photon searches, and future experiments should be able to probe a sizable fraction of the parameter space currently consistent with constraints. The latter model on the other hand is very difficult to probe experimentally, and its parameter space is largely unconstrained.

Chapter Four: Addressing Astrophysical and Cosmological Problems With Secretly Asymmetric Dark Matter[1]

Secretly Asymmetric Dark Matter (SADM) was proposed in the previous chapter as a mechanism to generate the dark matter (DM) relic abundance through an asymmetry in the dark sector despite an exact (global or gauged) DM number symmetry $U(1)_\chi$. In the implementation of this idea in ref. [54], the asymmetry is first generated in the visible sector through high-scale leptogenesis [38][2] and then transferred to a dark sector containing three DM flavors χ_i, a flavorless mediator ϕ, and a dark photon γ_D via a coupling to the right-handed leptons of the Standard Model (SM). The mediator in that case is charged both under SM hypercharge and under $U(1)_\chi$, and therefore leads to mixing between the photon and the dark photon at the one-loop level. This is phenomenologically only acceptable if the dark photon has a nonzero mass [94], and therefore the experimental signatures of the model manifest themselves at short distances, but in the context of long distance physics it falls under the collisionless cold DM category.

In this chapter we introduce a different implementation of the SADM mechanism, where a massless dark photon is phenomenologically allowed, and leads to a rich set of astrophysical signatures, despite the rather minimal high-energy setup. We argue that this setup is capable of addressing open questions in astrophysics both at the large (Hubble-scale) and small (galaxy-scale) scales simultaneously. The model we propose serves as a short-distance implementation of two mechanisms that have recently been proposed to address the same open questions, namely Dark Acoustic Oscillations [99, 95, 97, 96, 98] and Hidden Hydrogen DM [101, 102]. By focusing on a particular region of parameter space of the model, we show that the H_0 discrepancy [103], the σ_8 discrepancy [105, 106, 107, 108, 104] and the mass deficit problem [109, 104, 110] in dwarf galaxies and galaxy clusters can all be addressed. There have been many

---

[1]This chapter is based on work previously published as ref. [93]. This author contributed to the methodology, calculations, and text of this paper.

[2]See reviews of leptogenesis such as ref.s [73, 74] for a comprehensive list of references.

efforts in the literature to address these discrepancies using non-standard DM self interactions [111, 112, 114, 113, 115, 116, 117, 118, 119, 120]. The SADM model presented here extends these efforts by providing a minimal short-distance setup that nevertheless has rich enough dynamics to address multiple issues across a wide range of scales.

The core feature of the SADM mechanism is that due to the unbroken DM number symmetry, the total dark charge of the universe is zero at all times, but there can be several DM flavors that have individual asymmetries. Due to the crucial role of there being multiple DM flavors, SADM can be considered as a special case of the Flavored Dark Matter scenario [63, 21, 23, 64, 28, 72, 121]. Unlike the model studied in ref. [54] however, where the heavier DM flavors decay to the lightest one before Big Bang Nucleosynthesis (BBN) and result in a symmetric distribution of the lightest DM flavor at late times, in the model we study in this work all DM flavors are extremely long-lived and are still present today. This means that flavors with opposite signs of asymmetry (and with opposite dark charges) must coexist, along with a massless dark photon that mediates long-range interactions, and therefore multiple bound states can form, each one behaving as atomic DM [122, 123, 111]. These bound states, along with unbound DM particles and the massless dark photon then give rise to rich dynamics across a range of distance scales. The dark photon as an additional relativistic degree of freedom helps ease the tension between CMB-based [124] and low redshift [103, 126, 125] measurements of H_0, dark acoustic oscillations in the early universe that arise from the scattering of free and bound states leads to a suppression of the matter power spectrum at small scales, and the scattering between bound states after structure formation leads to a flattening of the DM density distribution inside haloes.

The layout of this chapter is as follows: In section 4.1 we introduce the short-distance model, and we consider its phenomenology in the context of particle physics observables and constraints. In section 4.2 we then study the cosmological features of the model, and the astrophysical signatures that it gives rise to at the large and small scales. We conclude in section 4.3 and we consider directions for future research.

4.1 The Model, and particle physics considerations

In this section we will introduce our SADM model and consider its high energy aspects. We assume heavy right handed neutrinos N_i exist and that they have Majorana masses as well as a Yukawa coupling to the SM leptons

$$\mathcal{L} \supset M_{N,ij} N_i N_j + Y_{ij}^N N_i \ell_j H^\dagger + \text{h.c.}, \tag{4.1}$$

where H is the SM Higgs doublet. This well-studied extension of the SM generates both light neutrino masses through the see-saw mechanism and it also allows the creation of a net $B - L$ number as the origin of the matter-antimatter asymmetry in the SM sector through CP violating phases in the coupling matrix Y_{ij}^N. These features are explored in depth in reviews of leptogenesis [73, 74].

To this setup we add three flavors of Dirac fermions $(\chi, \chi^c)_i$ and a scalar ϕ with the couplings (in the χ-mass basis)

$$\mathcal{L} \supset M_\phi^2 |\phi|^2 + m_{\chi,i} \chi_i^c \chi_i + \lambda_{ij} N_i \chi_j \phi + \text{h.c..} \tag{4.2}$$

Note that an exact $U(1)_\chi$ symmetry exists, under which all χ have charge +1, while all χ^c and ϕ have charge -1. We will take this symmetry to be gauged by the dark photon, with a fine structure constant α_d. The λ_{ij} coupling matrix contains physical phases and is a source of CP-violation in the dark sector. We choose the N to only couple to the left-handed χ (and ϕ) but not the right-handed χ^c (and ϕ^*). If couplings to both χ and χ^c are present with $\mathcal{O}(1)$ coefficients, this can allow a heavier χ particle to decay to a lighter one within the age of the universe, as will be discussed later in this section. While a coupling to χ^c will be generated through quantum effects, this effect is suppressed by ratio of χ and N masses, and this does not invalidate our estimate of the χ lifetime presented below. We will soon introduce a convention for assigning the flavor labels i.

The mediator ϕ, being a scalar, will be taken to be heavy, though we will assume that it is lighter than the right-handed neutrinos. Once the right-handed neutrinos become non-relativistic and the interaction of equation 4.2 drops out of equilibrium, the SM and dark sectors decouple from one another. As the heavy neutrinos N decay, they will then generate asymmetries both in the SM leptons and in the dark sector

(in ϕ and the χ_i); however as mentioned before $U(1)_\chi$ is never broken and therefore the total dark charge of the universe is zero at all times. With the interaction of equation 4.2 out of equilibrium, the asymmetries generated in the three χ flavors cannot wash each other out. As the temperature drops further, the ϕ particles become nonrelativistic and the symmetric part of the ϕ particle distribution annihilates to dark photons. The asymmetric ϕ particles then decay as $\phi \to \chi \ell^\pm H^\mp$, transferring their dark charge to the χ flavors, such that after the ϕ decays the asymmetry in the dark sector will reside entirely in the three DM flavors, in such a way that the total dark charge of the universe remains zero. Note that the heaviness of both ϕ and N means that the χ are very challenging to access in collider, direct detection, or indirect detection experiments. Our model does however have astrophysical signatures, which are the focus of this paper and which we will study in the next section.

Assuming generic phases in the entries of the Y_{ij}^N and the λ_{ij} matrices, the ratio of the typical magnitudes of the elements of Y_{ij}^N and the typical magnitudes of the elements of λ_{ij} will determine the branching ratio of the decaying N into the visible vs the dark sector, and thereby the ratio of the overall lepton number (more precisely, $B - L$ number) and the flavor-by-flavor χ asymmetries that are generated through heavy neutrino decays.

Therefore, for similar magnitudes in the entries of the Y_{ij}^N and the λ_{ij} matrices, the fact that $\Omega_{DM} \sim 5\Omega_B$ suggests the GeV scale for the mass of the heaviest χ flavor, but if the entries of one coupling matrix are larger than those of the other, then this mass can also vary in either direction. As we will show in section 4.2, the region of parameter space that is of interest for us has the mass of the heaviest DM flavor $\sim \mathcal{O}(10)$ GeV, the mass of the lightest DM flavor $\sim \mathcal{O}(1)$ MeV, and a value for α_d of order several percent. In this parameter region, the symmetric parts of the χ distributions annihilate efficiently, leaving behind only the asymmetric part generated during the N decays.

The asymmetry generated in the different χ flavors will differ from one another. In fact, due to the total dark charge of the universe being zero, there will always be one χ flavor with one sign of the asymmetry, and two flavors with the opposite sign, after the ϕ particles have all decayed. We will adopt the following naming convention for the three χ flavors: The χ flavor which is unique in its sign of the asymmetry will be labeled χ_1, whereas the two χ flavors with the other sign of the asymmetry will be labeled χ_2 and χ_3, such that $m_{\chi_2} > m_{\chi_3}$. As we will see in the next section, the
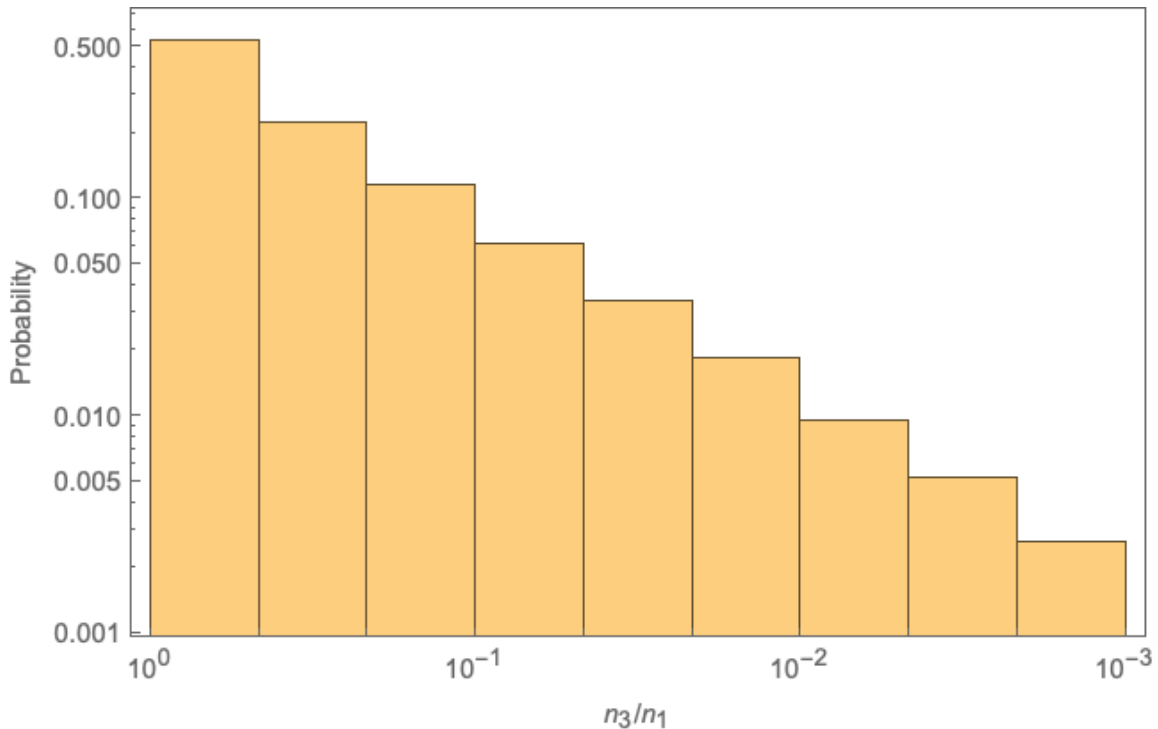
Figure 4.1: The estimate of the probability distribution function for the ratio n_3/n_1. See main text for the details of the calculation.

most interesting phenomenology is obtained when χ_3 and not χ_1 is the lightest DM flavor. Thus we will take $m_{\chi_1} > m_{\chi_3}$ as well, while either one of χ_1 or χ_2 could be the heaviest flavor. The possible bound states are then formed between χ_1 and χ_2, labeled H_{12}, and between χ_1 and χ_3, labeled H_{13}. Since the total dark charge of the universe is zero at all times, the asymmetries of χ_2 and χ_3 add up in magnitude to that of χ_1.

The overall size of the entries of the λ_{ij} coupling matrix determines the branching fraction of N to the dark sector, and therefore the overall size of the asymmetries of all χ flavors, while the specific flavor and phase structure in the coupling matrix determines the branching fractions among the DM flavors. The three comoving asymmetries ΔY_i of the χ flavors (after ϕ decays) satisfy $\sum_{i=1}^{3} \Delta Y_i = 0$. In terms of the physical number densities of the three χ particles (or antiparticles, depending on the sign of the asymmetry), this can also be written as $n_1 = n_2 + n_3$. Thus the n_i are not independent, however the ratio n_3/n_1 can in principle have any value in the interval

42

[0, 1].

We can estimate the probability distribution for this ratio using Monte Carlo methods with a prior where each entry of the 3×3 matrix λ_{ij} is randomly chosen over the unit complex circle. To calculate the asymmetry generated in each flavor from a given matrix λ_{ij}, we follow standard techniques from leptogenesis [73]. We assume the heavy neutrino masses are hierarchical with $m_{N_1} \ll m_{N_2}, m_{N_3}$ (we use $m_{N_1} = 1.0 \times 10^{16}$ GeV as a benchmark value). N_1 decays are fast compared to the Hubble scale, and therefore the asymmetry production takes place in the strong washout regime. Ratios of the ΔY_i generated in the N_1 decays can be obtained from the ratios of the CP asymmetry factors for each flavor i

$$\epsilon_{ii} \propto \text{Im}\{[\lambda]_{1i}[m^*\lambda]_{1i}\}, \tag{4.3}$$

where the matrix $[m]_{ij}$ is given by

$$[m]_{ij} = [\lambda]_{ki}[\lambda]_{kj}/m_{N_k}. \tag{4.4}$$

For the branching ratios of the subsequent ϕ decays, only the tree level contributions with an off-shell N_1 are used, since any additional CP violation introduced at this stage is subdominant. Note also that an *overall* rescaling of all λ_{ij} entries does not affect the probability distribution of n_3/n_1, and therefore we are not committing ourselves to a particular size of the λ_{ij} couplings by generating random numbers over the complex unit circle. For a given choice of m_{N_1} and m_{χ_i}, such a rescaling can be chosen such that the correct overall ρ_{DM} and ρ_B are obtained. The result for the n_3/n_1 probability distribution is shown in figure 4.1. As we will see in the next section, the region of greatest phenomenological interest corresponds to $n_3/n_1 \lesssim 0.1$, which does not require significant fine-tuning.

Even without a compressed spectrum among the DM flavors, all χ are extremely long-lived, and are still undecayed today. The leading decay mode arises from the one-loop diagram shown in figure 4.2. Let us estimate the lifetime associated with this decay mode. Since N is the heaviest particle in the spectrum, we integrate it out first. At dimension 5, this generates the operator (we use λ to stand in for any $\mathcal{O}(1)$ entries in the λ_{ij} coupling matrix, and we are suppressing flavor indices on the χ)

$$\mathcal{O}_5 = \frac{\lambda^2}{m_N} \left(\chi\chi\phi^2 + \text{h.c.} \right). \tag{4.5}$$
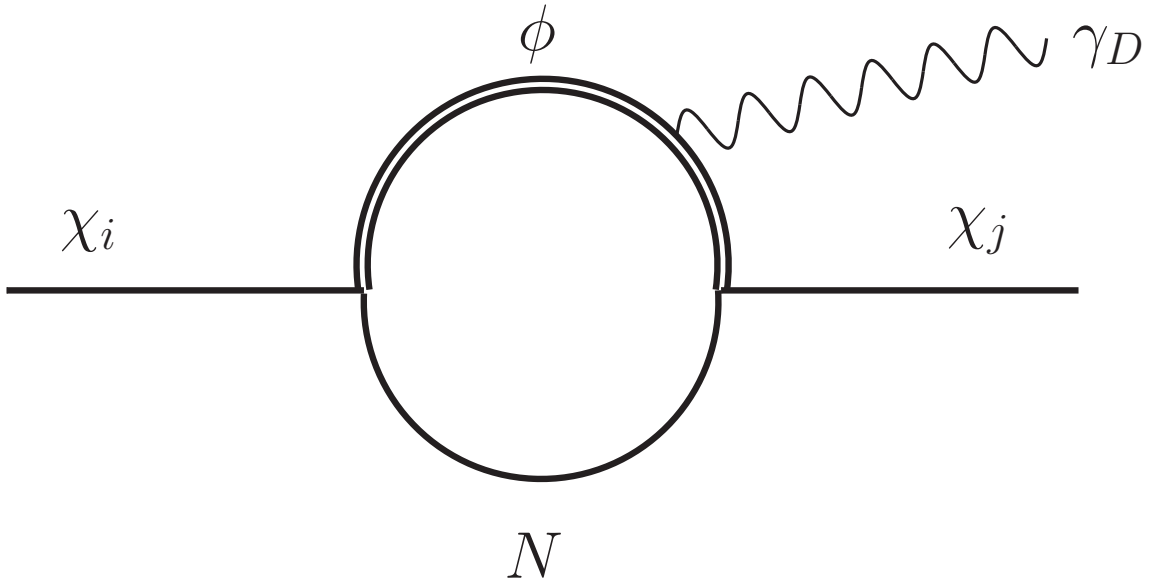
Figure 4.2: Decay mode for a heavier DM flavor to decay to a lighter one.

Note however that this operator does not contribute to the decay mode of figure 4.2, since one needs a factor of $\phi\phi^*$ in order to close the ϕ loop. In order to do this, we need to go to the dimension 6 operator generated from integrating out N

$$\mathcal{O}_6 = \frac{\lambda^2}{m_N^2} \left(\bar{\chi}\bar{\sigma}^\mu \partial_\mu \chi \phi\phi^* \right). \tag{4.6}$$

Next, we will integrate out the heavy mediator ϕ. In the low energy theory below m_ϕ, the effective operator that leads to the χ decay is the operator

$$\bar{\chi}\bar{\sigma}^\mu \partial^\nu \chi \, F_{d\,\mu\nu}, \tag{4.7}$$

where $F_{d\,\mu\nu}$ is the field strength for $U(1)_\chi$. Since all derivatives in this effective operator act on the external momenta, which are of order m_χ, the decay rate can be estimated as

$$\Gamma_{\text{approx.}} = \frac{1}{8\pi} \left(\frac{\lambda^2 e_d}{16\pi^2 m_N^2} \right)^2 m_\chi^5 \tag{4.8}$$

We have also performed the full loop calculation for this process, and we find complete agreement with the effective field theory estimate presented above, with an added numerical factor of 1/72. The full answer for the decay rate is thus found to be, up
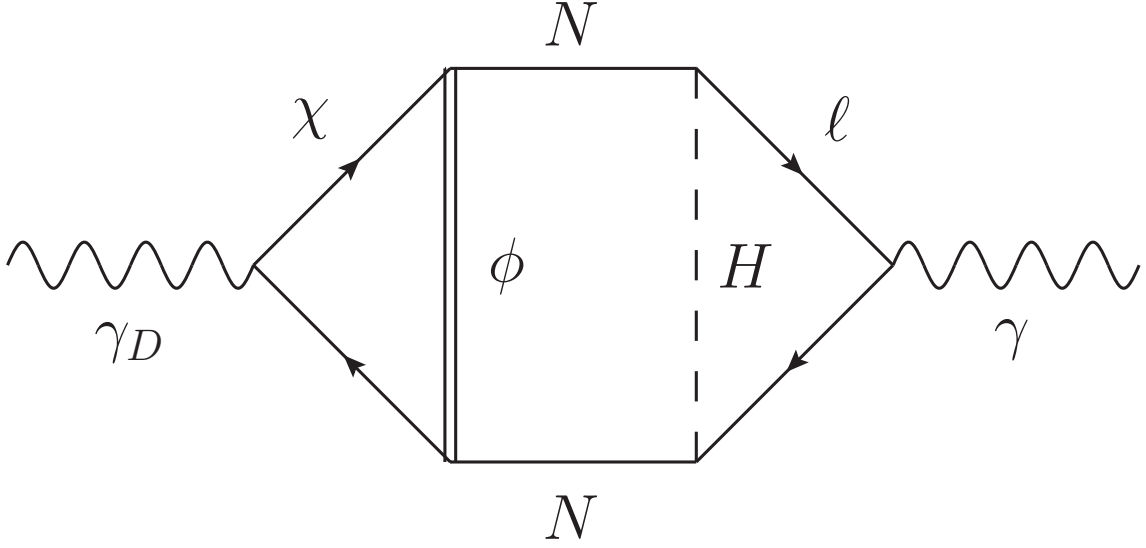
Figure 4.3: Leading contribution to mixing between the dark photon and the SM photon.

to corrections of order $\left(m_\phi^2/m_N^2\right)$ and of order $\left(m_{\chi,\text{final}}^2/m_{\chi,\text{initial}}^2\right)$:

$$\Gamma = \frac{1}{72}\Gamma_{\text{approx.}} \tag{4.9}$$

$$\approx (10^{-42}\text{eV})\left(\lambda^4 e_d^2\right)\left(\frac{m_\chi}{10\text{GeV}}\right)^5\left(\frac{10^{12}\text{GeV}}{m_N}\right)^4 \tag{4.10}$$

$$\ll H_0 \approx 10^{-33} \text{ eV}. \tag{4.11}$$

The lifetime is several orders of magnitude larger than the age of the universe for the parameter region that will be used in this paper. The leading tree-level decay diagrams are even further suppressed than this decay mode, and are therefore irrelevant. As discussed earlier in this section, if the UV theory contains couplings of N to both χ and χ^c with $\mathcal{O}(1)$ coefficients, then the operator $\mathcal{O}_5$ of equation 4.5 will contain a cross-term containing $\chi\chi^c\phi\phi^*$ which can contribute to the decay process at order $1/m_N$ instead of at order m_χ/m_N^2, leading to an unacceptably short lifetime. If the coupling to χ^c is absent in the UV theory however, it is only generated with an m_χ/m_N suppression, and this contributes at the same order as the piece already considered in equation 4.9.

As we will see in the next section, the most interesting phenomenological features

of the model will be obtained when the mass of the heaviest flavor (χ_1 or χ_2) is $\mathcal{O}(10)$ GeV, the mass of the next heaviest flavor is $\mathcal{O}(0.1 - 1)$ GeV, and the mass of the lightest flavor (χ_3) is $\mathcal{O}(1)$ MeV. This means that H_{12} will be strongly bound and difficult to ionize, serving as a neutral DM component, while H_{13} may be easy to ionize, such that a non-negligible fraction of χ_3 (and the corresponding amount of χ_1) can be unbound at certain times during the early universe, delaying the decoupling of the dominant DM component from the dark radiation, and leading to interesting dynamical effects.

For a massless dark photon, it needs to be checked that the mixing with the SM photon is acceptably small. More precisely, in the basis where γ_D only interacts with χ but not the SM fermions, the millicharge acquired by χ under electromagnetism needs to be small. The γ-γ_D mixing is induced at the three-loop level: see figure 4.3. Matching on to an effective operator $\epsilon F_D^{\mu\nu} F_{\mu\nu}$, one can estimate

$$\epsilon \sim \frac{e e_D \lambda^2 Y^2}{(16\pi^2)^3}. \tag{4.12}$$

If $\lambda^2 \sim Y^2 \sim 0.1$ and $\alpha_d \sim \alpha$, then ϵ is below 10^{-10}. Let us compare this to the constraints for millicharged DM (figure 1 in ref. [127], with $m \sim \mathcal{O}(10)$ GeV, the mass of the heaviest DM flavor), keeping in mind that some of the constraints will be relaxed, as these were derived with the assumption that all DM particles are millicharged while we will focus in this work exclusively on the possibility that all but a small fraction of the χ particles are in bound states, and therefore have no *net* millicharge. In particular, the leading constraints from galactic and cluster magnetic fields probe the DM at small momenta, or at distance scales larger than the size of the bound states, thus these constraints cannot resolve the millicharges of the constituents. While the momentum scale that is probed at LUX is still too small to resolve the constituents of H_{12}, it may be sufficiently large to resolve the constituents of H_{13}. However, in the parameter space of interest to us, H_{13} is the subdominant DM component, which relaxes the constraints below the generic values of ϵ in our model. Furthermore, for a significant fraction of the parameter region of interest to us (especially when $m_{\chi_2} > m_{\chi_1}$), the mass of H_{13} is below the sensitivity of LUX. It is however interesting to note that future direct detection experiments with a low mass threshold may be able to test the scenario presented here. Finally, for the parameter region of interest, the value of ϵ in our model is also below the bounds from supernovae [94].

As a final consideration about the particle physics nature of our model, we want to address the potential concern that flavor oscillations between the DM flavors may cause a washout of the asymmetries, as the particles of χ_1 oscillate into the antiparticles of χ_2 or χ_3, or the other way around. However, the large mass gap between the χ flavors in the parameter region of interest in this chapter, and the extremely small intrinsic widths of these states makes oscillations so small that they are negligible for all intents and purposes.

4.2   Cosmology and astrophysical signatures

Having discussed the short-distance physics aspects of our model, we now turn our attention to the role it plays in the dynamics of the early universe, as well as in late-time astrophysical processes. Although the dark sector is hidden from direct experimental probes via non-gravitational interactions, the dynamics within the SADM sector can significantly change the gravitational potential in the early universe and it leaves visible signals on both the large and small scale structures. We will show that there is a region of parameter space where observational anomalies on scales of dwarf galaxies ($\sim$ kpc size) [109, 104], galaxy clusters ($\sim$ Mpc size) [110], the σ_8 problem ($\sim$ 10 Mpc size) [105, 106, 107, 108, 104], and the tension in the measurements of H_0 from the CMB [124] and from low redshift measurements [128] may all be addressed.

The input parameters of the model that are relevant at large distances can be listed as the comoving asymmetries of the χ flavors (of which only two are independent, and which can therefore be parameterized in terms of n_1 and n_3/n_1 once the symmetric part of the χ distributions annihilates away), the masses of the three χ flavors, and α_d. In order to calculate how the temperature of the dark sector is related to that of the SM sector, consider energies above m_N where the interaction of equation 4.2 keeps the two sectors in equilibrium. As the temperature drops below m_N, the visible and dark sectors decouple. At this time, the dark sector contains the three Dirac fermions $\chi_{1,2,3}$, the complex scalar ϕ, and the dark photon γ_D. ϕ is only somewhat lighter than the N, and for the parameter region of interest for us, the mass of the lightest flavor is $\mathcal{O}(1)$ MeV. Therefore, at the time of structure formation, only γ_D is still relativistic.

If there are no other degrees of freedom in the visible sector other than those of the SM up to energies of m_N, then by using the ratio of the number of relativistic degrees

of freedom in the two sectors at the decoupling scale and at the scale of structure formation, one obtains $\Delta N_{eff} = 0.75$. However, since the two sectors decouple at a very high temperature scale, one needs to take into account the possibility that the visible sector contains additional degrees of freedom (e.g. connected to the solution of the electroweak naturalness problem, grand unification, etc.) that release additional entropy in the visible sector as the universe cools down, and thereby further suppress ΔN_{eff}. The value 0.75 should therefore be considered as an upper limit, with the actual value depending on other possible extensions of the SM. Since a value of 0.75 is outside the 2σ contour for reconciling the H_0 discrepancy (see e.g., [124]), we will adopt a benchmark value of $\Delta N_{eff} = 0.60$ for the remainder of the paper[3], which can be obtained for example if there are six Dirac fermions beyond the SM in the visible sector. Adding even more degrees of freedom to the visible sector would further reduce ΔN_{eff}. It should also be noted that at the time of BBN, ΔN_{eff} is even smaller ($\Delta N_{eff} = 0.42$) since χ_3 has not yet become nonrelativistic at that time for $m_{\chi_3} \lesssim$ MeV, which is the preferred value for addressing the σ_8 problem as we will see later. Thus our model is compatible with BBN constraints [131].

There are two recombination processes during the early universe, of χ_1 with χ_2 into H_{12}, and of the remaining χ_1 with χ_3 into H_{13}. H_{12} forms earlier due to its larger binding energy, and the remaining χ_1 and χ_3 particles scatter with each other and remain in thermal equilibrium at this time. Similar to the proton-hydrogen scattering in the SM, the scattering cross section between the non-relativistic χ_1 and the H_{12} bound state is sufficient for keeping them in thermal equilibrium with each other. In the scenario we are interested in, the momentum transfer q necessary to keep H_{12} in thermal equilibrium at a dark temperature $T_d \sim 10$ eV during the dark acoustic oscillations is given by $q \sim \sqrt{m_{\chi_1} T_d} \sim 10^{4.5}$ eV, which is much smaller than the inverse size $a_0^{-1} \sim (\alpha_d m_{\chi_2}) \sim 10^7$ eV of the H_{12} bound state (for $m_{\chi_2} \sim$ GeV). In this limit, the scattering rate of H_{12} and χ_1 can be estimated as $\sigma v_{\chi_1} n_{\chi_1} \sim 4\pi \alpha_d^2 m_{\chi_2}^2 a_0^4 \sqrt{T_d/m_{\chi_1}} n_{\chi_1} \sim 10^{-26}$ eV [111], which exceeds the Hubble expansion rate at that time. We therefore treat H_{12}-χ_1 to be in thermal equilibrium during the acoustic oscillations. While χ_1-χ_3 scattering is also efficient, the entire dark sector is then in thermal equilibrium with the dark photon, and the resulting DM oscillations delay the formation of large scale structure.

---

[3]According to Fig. 35 in [124], this rather large ΔN_{eff} is within 2σ constraint from the joint Planck TT,TE,EE+lowE+lensing+BAO fit including the low redshift measurement [129].

The oscillation stops as H_{13} recombines, which leaves too few free (dark-)charged particles to sustain the oscillations. These dark acoustic oscillations generate a small but visible damping of the matter power spectrum and may provide a solution to the σ_8 problem. A more complete parameter fitting procedure including also the CMB and BAO data is necessary to confirm this claim in full detail, however in this work we will take a simpler approach and we will calculate the size of power spectrum suppression to argue that the claim is plausible, leaving a more detailed analysis to future work.

We will also show that at later times, during the formation of DM halos, the scattering between H_{12} bound states leads to thermal equilibrium and provides a solution to the core/cusp problem of dwarf galaxies. The non-trivial velocity dependence due to the inelastic scattering $H_{12}H_{12} \rightarrow H_{12}H_{12}\,\gamma_D$ through the dark hyperfine transition also gives the right cross section for cores to form in relaxed cluster halos. As we will see, achieving this will favor the parameter region where the heaviest DM flavor mass is $\sim \mathcal{O}(10)$ GeV, where the value of α_d is a few percent, and $n_3/n_1 \sim 0.1$. Furthermore, we will see that achieving the correct amount of damping of large scale structure favors the MeV range for $m_{\chi 3}$. Thus there is a region of the parameter space of our model where all parameters are technically natural and where all three structure formation problems (dwarf, cluster and σ_8) and the H_0 tension could be addressed. Below, we explore each of these aspects of our model in detail.

4.2.1   Dark recombination(s)

The formation of the H_{12} and H_{13} bound states plays an important role in structure formation. In particular dark acoustic oscillations end when there are no longer sufficiently many unbound χ particles left to sustain them. Similar to the recombination of hydrogen in the SM, for both H_{12} and H_{13}, recombination proceeds through the formation of the excited states ($n \geq 2$), with a subsequent decay into the ground state either through a two photon emission or through a Lyman-α transition, where the dark photon becomes redshifted before ionizing other bound states.

A brief note on notation: we have introduced n_i in the previous section to denote the physical densities in each flavor. Since in this section we will also need to keep track of just the density of unbound particles in each flavor, we will introduce the notation n_i^f, where f stands for "free". With this definition $n_1 = n_1^f + n_{H_{12}} + n_{H_{13}}$,

$n_2 = n_2^f + n_{H_{12}}$ and $n_3 = n_3^f + n_{H_{13}}$. We also define the ionization fraction in each flavor as $X_i \equiv n_i^f/n_i$. Note that the dark charge neutrality of the universe enforces both $n_1 = n_2 + n_3$ and also $n_1^f = n_2^f + n_3^f$.

The Boltzmann equation for $X_{2,3}$, can be written as [102]

$$\frac{dX_{2,3}}{dt} = C_{2,3}\left\{(1 - X_{2,3})\beta_{2,3} - X_{2,3}\, n_1^f \alpha_{2,3}^{(2)}\right\}, \quad \beta_{2,3} \equiv \alpha_{2,3}^{(2)} \left(\frac{m_{2,3}\, T_d}{2\pi}\right)^{3/2} e^{-\epsilon_{2,3}/T_d}. \tag{4.13}$$

Here, T_d stands for the temperature of the dark photon bath, and $\epsilon_{2,3}$ stands for the binding energy of H_{12} and H_{13}, respectively, given by $\mu\, \alpha_d^2/2$, with μ the reduced mass of the bound state in question. $\beta_{2,3}$ is the recombination rate, which relates to the ionization rate of the excited ($n = 2$) state

$$\alpha_{2,3}^{(2)} = 9.78 \frac{\alpha_d^2}{m_{\chi_{2,3}}^2} \left(\frac{\epsilon_{2,3}}{T_d}\right)^{1/2} \ln\left(\frac{\epsilon_{2,3}}{T_d}\right). \tag{4.14}$$

The factor $C_{2,3}$ takes into account Peebles' correction to the process, and its value can be approximated as

$$C_{2,3} = \frac{\Lambda_{\alpha(2,3)} + \Lambda_{2\gamma_D(2,3)}}{\Lambda_{\alpha(2,3)} + \Lambda_{2\gamma_D(2,3)} + \beta_{2,3}^{(2)}}, \quad \Lambda_{\alpha(2,3)} = \frac{H(3\,\epsilon_{2,3})^3}{(8\pi)^2 n_{2,3}(1 - X_{2,3})}, \tag{4.15}$$

with H being the Hubble rate. $\Lambda_{2\gamma_D(2,3)}$ stands for the two photon decay rates of H_{12} and H_{13}. We estimate the two photon decay rate in our model by rescaling the SM rate $\Lambda_{2\gamma} = 8.227$ sec^{-1}. As given in equation 2 of [130], the parametric dependence of this rate is given by the ground state energy times α^6, and we substitute the corresponding values of these quantities in our model to obtain $\Lambda_{2\gamma_D(2,3)}$. The Lyman alpha production rate is $\beta_{2,3}^{(2)} = \beta_{2,3}\, e^{3\epsilon_{2,3}/4T_d}$. When calculating the ionization fractions, we calculate the Hubble expansion rate, keeping in mind that the dark and visible sectors have different temperatures, using the benchmark value $\Delta N_{eff} = 0.60$ as discussed above.

In Fig. 4.4, we plot X_3 during H_{13} recombination, for a few representative values of m_{χ_3} and α_d, for $n_3/n_1 = 10\%$. The plots on the left and right correspond to the case where χ_1 is the heaviest flavor with $m_{\chi_1} = 25$ GeV, and the case where it is the second heaviest flavor with $m_{\chi_1} = 1$ GeV, respectively. The relic ionization fraction becomes larger either for a smaller value of α_d or a larger value of m_{χ_3}. The residual ionization fraction can be approximated as [99]

$$X_3 \sim 3 \times 10^{-6} \left(\frac{T_d}{T_\gamma}\right) \left(\frac{\alpha_d}{0.02}\right)^{-6} \left(\frac{n_1}{n_3}\right) \left(\frac{m_{H_{13}}}{\text{GeV}}\right) \left(\frac{\epsilon_3}{\text{keV}}\right). \tag{4.16}$$
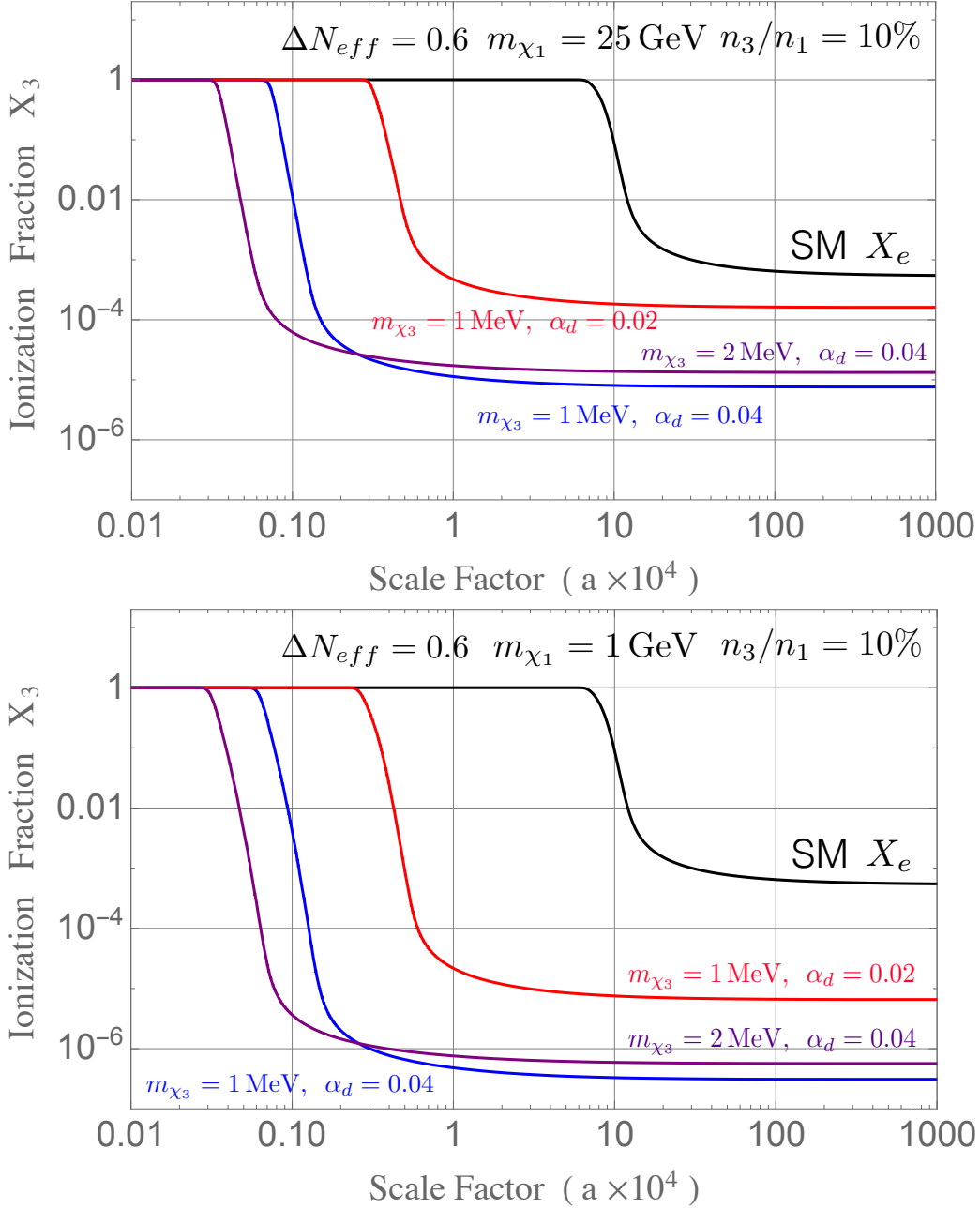
Figure 4.4: The SM (black) and χ_3 ionization fractions during the recombination epoch as a function of the scale factor, for representative values of (m_{χ_3}, α_d) and two χ_1 masses corresponding to the cases where χ_1 is the heaviest DM flavor (left), and the second heaviest DM flavor (right).

Dark baryon acoustic oscillations end after H_{13} recombination, and the recombination time scale determines the suppression of the power spectrum. Since the H_{12} recombination happens at a much earlier time, it does not have a strong effect on the power spectrum.

4.2.2   Dark acoustic oscillations and large scale structure

We now turn our attention to the evolution equations for the DM and dark radiation (DR) density perturbations in our model, after the H_{12} recombination, but before the H_{13} recombination. Thus the relevant matter degrees of freedom are χ_1 (with $X_1 \sim n_3/n_1$ during this epoch), χ_3 (with $X_3 \sim 1$) and the bound state H_{12} (with $n_{H_{12}} \sim n_2$). As discussed earlier in this section, we treat all the dark matter particles to behave as a single fluid during the dark acoustic oscillations and refer to these degrees of freedom collectively as "Acoustic DM" (AcDM) that undergo acoustic oscillations. We work in the conformal Newtonian gauge [133]

$$ds^2 = a^2(\tau) \left[-(1+2\psi)d\tau^2 + (1-2\phi)\delta_{ij}dx^i dx^j \right], \tag{4.17}$$

where the fields ψ and ϕ describe scalar perturbations on the background metric. To linear order in the perturbations, we have

$$\dot{\delta}_{\text{AcDM}} = -\theta_{\text{AcDM}} + 3\dot{\phi}, \tag{4.18}$$

$$\dot{\theta}_{\text{AcDM}} = -\frac{\dot{a}}{a}\theta_{\text{AcDM}} + \frac{4\rho_{\gamma_D}}{3\rho_{\text{AcDM}}} n_3^f(a)\sigma_T \, a(\theta_{\gamma_D} - \theta_{\text{AcDM}}) + k^2\psi, \tag{4.19}$$

where the derivatives are with respect to η, the conformal time. $\delta \equiv \delta\rho/\bar{\rho}$ is the perturbation of the energy density, k is the wave number, and $\theta \equiv \partial_i v^i$ is the divergence of the comoving 3-velocity. Since the AcDM components are all non-relativistic at this time, one can ignore the sound speed[4]. As long as the momentum transfer rate from the dark Thomson scattering $\gamma_D \chi_3 \to \gamma_D \chi_3$ is comparable to Hubble, the density perturbations oscillate with the dark photon perturbation, and structures cannot grow. The cross section is given by $\sigma_T = 8\pi\alpha_d^2/3m_{\chi_3}^2$, and n_3^f depends on the ionization fraction X_3 obtained by solving Eq. (4.13). The dark photon perturbations,

---

[4]We have verified numerically that this gives a good approximation.

including higher modes in the Legendre polynomials, $F_{\gamma_D \ell}$, evolve as [133]

$$\dot{\delta}_{\gamma_D} = -\frac{4}{3}\theta_{\gamma_D} + 4\dot{\phi}, \tag{4.20}$$

$$\dot{\theta}_{\gamma_D} = k^2 \left(\frac{1}{4}\delta_{\gamma_D} - \frac{1}{2}F_{\gamma_D 2}\right) + a\, n_3^f\, \sigma_T(\theta_{\mathrm{AcDM}} - \theta_{\gamma_D}) + k^2\psi, \tag{4.21}$$

$$\dot{F}_{\gamma_D 2} = \frac{8}{15}\theta_{\gamma_D} - \frac{3}{5}kF_{\gamma_D 3} - \frac{9}{10}a\, n_3^f\, \sigma_T F_{\gamma_D 2}, \tag{4.22}$$

$$\dot{F}_{\gamma_D l} = \frac{k}{2l+1}\left[lF_{\gamma_D(l-1)} - (l+1)F_{\gamma_D(l+1)}\right] - a\, n_3^f\, \sigma_T F_{\gamma_D l}, \quad l \geq 3 \tag{4.23}$$

$$\dot{F}_{\gamma_D l_{\max}} = kF_{\gamma_D(l_{\max}-1)} - \frac{l_{\max}+1}{\tau}F_{\gamma_D l_{\max}} - a\, n_3^f\, \sigma_T F_{\gamma_D l_{\max}}. \tag{4.24}$$

Here the $F_{\gamma_D l}$ are related to the spatial variations in the density fluctuations in the dark photons, in particular $\delta_{\gamma_D} \equiv F_{\gamma_D 0}$, $\theta_{\gamma_D} \equiv \frac{3}{4}kF_{\gamma_D 1}/4$, and $\sigma \equiv \frac{1}{2}F_{\gamma_D 2}$ where σ is the shear stress. We truncate the Boltzmann hierarchy at order $l_{\max} = 4$, making use of the approximation outlined in Ref. [133][5]. The equations are similar to those for the SM photon and baryons.

In the calculation we take $\psi = \phi$ and ignore the correction from free streaming radiation. This approximation is good since our ΔN_{eff} is much smaller than the number of light neutrinos. Gravity perturbations are sourced by the density fluctuations as described by the Einstein equation,

$$k^2\psi + 3\frac{\dot{a}}{a}\left(\dot{\psi} + \frac{\dot{a}}{a}\psi\right) = -\frac{a^2}{2M_{pl}^2}\sum \rho_i\, \delta_i, \tag{4.25}$$

where the sum is over the SM photon, the dark photon and the AcDM components. For the initial conditions, the modes that enter the horizon before matter-radiation equality satisfy

$$\delta_{\gamma_D} = \frac{4}{3}\delta_{\mathrm{AcDM}} = -2\psi, \quad \theta_{\gamma,\gamma_D,\mathrm{AcDM}} = \frac{k^2\eta}{2}\psi, \tag{4.26}$$

and the modes that enter during the era of matter domination satisfy

$$\frac{3}{4}\delta_{\gamma_D} = \delta_{\mathrm{AcDM}} = -2\psi, \quad \theta_{\gamma,\gamma_D,\mathrm{AcDM}} = \frac{k^2\eta}{3}\psi. \tag{4.27}$$

We set the initial values of the higher modes $F_{\gamma_D \ell \geq 2} = 0$, since these higher angular modes quickly damp away when the AcDM-γ_D scattering is efficient. We neglect the

---

[5]We have also reproduced the analysis with $l_{\max} = 5$ to confirm that our results are not sensitive to the choice of $l_{\max}$.

tilt in the primordial spectrum ($n_s = 1$) and take a k-independent value of $\psi = 10^{-4}$. The final results are independent of the precise value of ψ since we are interested in the ratio of the matter power spectra with and without the dark acoustic oscillations. In the numerical study, we choose the values $h = 0.67$, $\Omega_\gamma h^2 = 2.47 \times 10^{-5}$, $\Omega_\Lambda h^2 = 0.69$, $\Omega_b h^2 = 2.2 \times 10^{-2}$, and $\Omega_\nu = 0.69 \Omega_\gamma$ [124].

After solving this set of differential equations, in order to quantify the importance of dark acoustic oscillations, we compare the DM power spectrum of AcDM to that of collisionless DM with an added non-interacting dark photon component, such that the energy density of dark radiation is equal in both scenarios, and further complications in the fitting of cosmological parameters are avoided:

$$\frac{P(k)_{\text{AcDM}}}{P(k)_{\Lambda\text{CDM+DR}}} \approx \left(\frac{\delta_\chi(k)_{\text{AcDM}}}{\delta_\chi(k)_{\Lambda\text{CDM+DR}}} \right)^2, \tag{4.28}$$

where the terms on the right hand side refer only to the nonrelativistic DM component. We show the power spectrum ratio in Fig. 4.5 for two representative values of α_d in the region of interest. When the H_{13} recombination takes place, the momentum transfer term in Eq. (4.19) quickly drops blow the Hubble expansion rate. The density perturbations entering the horizon after this point evolve the same way as they would in the ΛCDM scenario, and thus the ratio for small k modes asymptotes to 1. The matter power spectrum receives a suppression for modes that enter the horizon before recombination, thus for a lower H_{13} binding energy (blue curve) there is a larger suppression. This helps to explain the results of low red-shift measurements for σ_8. We estimate the viable parameter region by requiring a $5 - 15\%$ suppression of the power spectrum at $k = 0.2\,h$ Mpc^{-1} (blue band in figure 4.5 and yellow band in figure 4.6). Although in this work we only focus on the suppression of the matter power spectrum in the linear regime, the suppression continues past $k = 0.2h$ Mpc^{-1}. One thing to notice is that unlike the warm dark matter scenario that can totally eliminate the matter power spectrum at small scales, the suppression due to the dark acoustic oscillations itself oscillates before entering the non-linear regime. As is shown, e.g., in Ref. [134, 135], the gravitational collapse after redshift $z \lesssim 10$ is likely to destroy this oscillation pattern and therefore it reduces the suppression of the power spectrum in the non-linear region. Once the non-linear corrections to the density perturbation are included, the galaxy survey data and Lyman-α observations, which probe the matter power spectrum at even larger k-modes, can be used
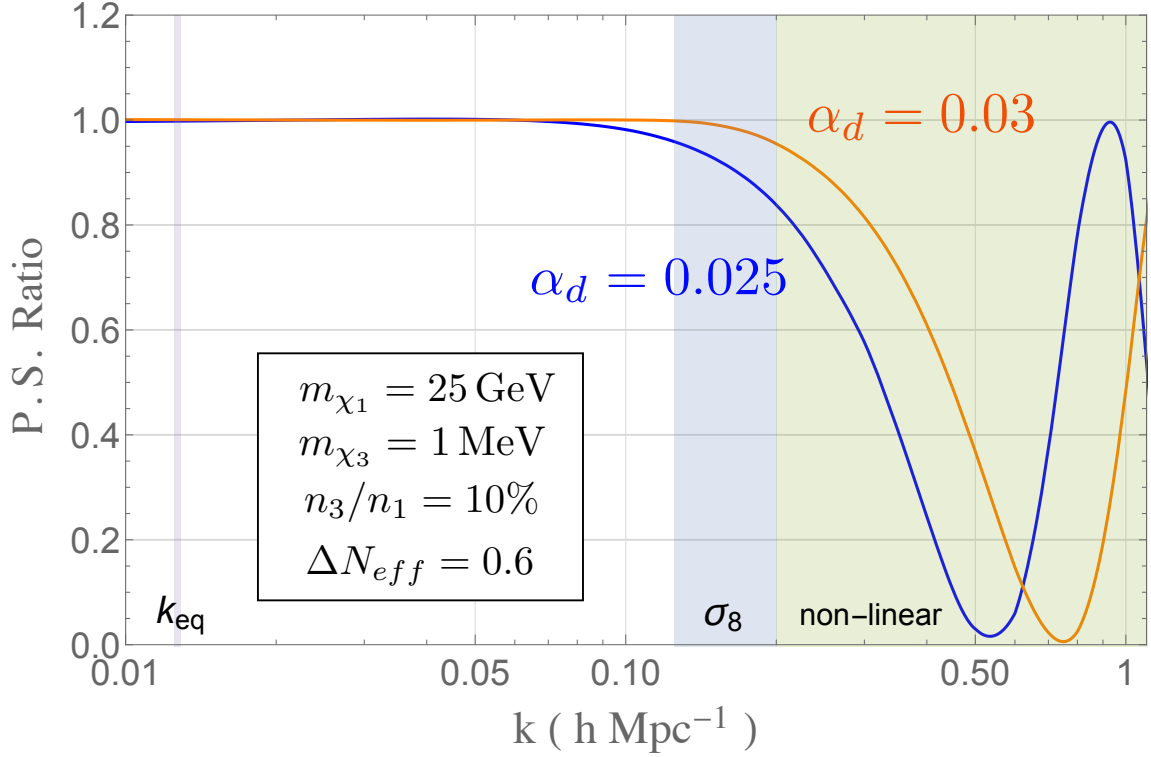
Figure 4.5: Ratio of the matter power spectrum between scenarios with and without dark acoustic oscillations, as is defined in Eq. (4.28). We use two representative values of α_d in the region of interest. The result is obtained by solving the linear order equations listed in the text. The ratio at large k is expected to receive further corrections from non-linear effects.

to further constrain dark acoustic oscillations [100, 136, 137, 138], and thereby the parameter space of our model.

4.2.3 Scattering between bound states and small scale structure

After halo formation, the scattering cross section between the non-relativistic H_{12} bound states in the halo is roughly geometric in size, $\sigma \sim (\mu_{12}\alpha_d)^{-1}$. For the region of parameter space we are interested in, where the heaviest DM flavor has a mass of $\mathcal{O}(10)$ GeV and $\alpha_d \sim 10^{-2}$, the resulting cross section over mass ratio $\sigma/m_{H_{12}} \sim 0.1$ cm^2/g can be large enough to thermalize the bound states and change the DM density

in the inner part of the halo. It was pointed out in Ref. [101] that dark hydrogen with a similar range of mass and couplings can explain the low DM density cores observed in small galaxies. Moreover, if the hyperfine splitting of the bound state

$$E_{hf} = \frac{8}{3} \alpha_d^2 f(R)^{-1} E_0, \quad R \equiv \frac{m_{\chi 1}}{m_{\chi 2}}, \quad f(R) = R + 2 + R^{-1} - \frac{\alpha_d^2}{2} \quad (4.29)$$

normalized by the energy scale $E_0 = \alpha_d^2 \mu_{12}$ is comparable to the kinetic energy of the bound state, the effect of the inelastic hyperfine upscattering is to enhance the cross section of H_{12} self-interactions. The velocity dependence in this process makes the self-interaction cross sections in dwarf halos larger than that in cluster halos, giving the correct σ/m ratio to solve the mass deficit problem in galaxy clusters.

In order to show that the same mechanism also works in the region of parameter space that is of interest to us, we adopt the best fit value from ref. [101]

$$E_{hf} = 10^{-4} E_0 \quad (4.30)$$

and we limit ourselves to the range of α_d in Fig. 3 of [101], where both the dwarf and cluster data can be explained. Since we want the H_{12} self-interaction to solve the small scale structure problem, we choose $n_3/n_1 = 0.1$ as our benchmark value such that H_{12} and not H_{13} is the dominant component of DM, while the n_3 number density is not unnaturally small (see figure 4.1), and also not too small to maintain the thermal equilibrium in the early universe that is responsible for suppressing structure formation and addressing the σ_8 discrepancy.

Even though it constitutes a smaller fraction of the DM energy density, we need to assess whether the H_{13} bound state may still play a role in halo formation. In particular, the H_{13} bound state has a much larger radius than H_{12} due to the smallness of $m_{\chi 3}$, and therefore scattering with H_{13} could potentially change the desired core size of the H_{12} halo. However, we find that this is not the case. For the parameter range we consider, the inverse Bohr radius of H_{13} (~ 10 keV) is still too small compared to to the value that would result in sufficient momentum transfer for keeping H_{12} atoms in thermal equilibrium both at dwarf galaxies ($\sim$ MeV) and galaxy clusters (~ 100 MeV). Thus the scattering process most efficient for momentum transfer is off the χ_1 particle (i.e. the "nucleus") inside H_{13}, with a cross section comparable to the H_{12} self-scattering. Therefore the geometric size of H_{13} does not lead to an enhancement, and the H_{12} isothermal profile is not significantly affected.

As structures form, the bound states fall into the overdense region and their gravitational potential energy is converted into kinetic energy, resulting in shock-heating to a temperature [139]

$$T_{gal} \approx 0.86 \, \text{keV} \frac{\mu}{10 \, \text{GeV}} \tag{4.31}$$

for a Milky Way sized galaxy with halo mass $10^{12} M_\odot$ and radius 110 kpc. Here μ is the total mass of all degrees of freedom that contribute to ρ_{DM} divided by their total number density, given by

$$\mu = \frac{(n_2 - n_2^f)m_{H_{12}} + (n_3 - n_3^f)m_{H_{13}} + \sum_{i=1}^{3} n_i^f m_{\chi_i}}{(n_2 - n_2^f) + (n_3 - n_3^f) + \sum_{i=1}^{3} n_i^f}. \tag{4.32}$$

If T_{gal} is higher than the binding energy, bound states can dissociate. While the more tightly bound H_{12} does not dissociate in the region of parameter space that is of interest to us, if H_{13} "reionizes" in this fashion, the scattering process $\chi_3 \chi_1 \to \chi_3 \chi_1 \gamma_D$ can lead to efficient cooling through bremsstrahlung. For simplicity, when checking for the ionization of H_{13}, we take the initial condition to be $n_i^f = 0$. In the parameter region where H_{13} reionizes, we then recalculate T_{gal} with $n_1^f = n_3^f = n_3$ (fully reionized H_{13}) to use in the estimate for the cooling process. An estimation of the cooling time scale through this process is given by [139]

$$t_{brem} \sim 6 \, \text{Gyr} \left(\frac{0.02}{\alpha_d}\right)^3 \left(\frac{0.1}{n_3/n_1}\right) \left(\frac{\mu}{10 \, \text{GeV}}\right)^{\frac{1}{2}} \left(\frac{m_{H_{12}}}{10 \, \text{GeV}}\right) \left(\frac{m_{\chi_3}}{1 \, \text{MeV}}\right)^{\frac{3}{2}}. \tag{4.33}$$

The emitted dark photon can have a free streaming length much larger than the size of the halo, leading to halo cooling. If t_{brem} is much shorter than the age of the Milky Way (T_{MW}), a dark disc may form. Recently, results from the GAIA survey [140] have been used to set an upper bound on the fraction of the DM that can be contained in a dark disc at $\sim 1\%$ [141, 142]. A detailed study of the cooling process and the merger history of sub-halos is beyond the scope of this work, therefore as we scan through the parameter space of our model, we will use t_{brem}/T_{MW} as a conservative indicator of whether there is a significant probability of dark disc formation. In Fig. 4.6, the region where H_{13} can be reionized due to shock heating is shown below the red-dotted curve, and the region where the condition for efficient bremsstrahlung cooling is satisfied is shown above the red dashed curve, resulting in the red shaded region where both conditions are satisfied and where a dark disc may form.

4.2.4 Reconciling the large and small scale structure problems

In figure 4.6, we show our combined results for several representative parameter choices, and as a function of m_{χ_3} and α_d. As mentioned in the previous section, we fix $n_2/n_1 = 0.9$. We consider 25 GeV and 45 GeV as the mass of the heaviest DM flavor, considering both possible hierarchies, $m_{\chi_1} > m_{\chi_2}$ and $m_{\chi_2} > m_{\chi_1}$.

- **Addressing the σ_8 discrepancy:** We calculate the power spectrum ratio of Eq. (4.28) for $k = 0.2h$ Mpc^{-1}, which is close to the perturbation mode for the σ_8 measurement. The contours of the power spectrum suppression depend mainly on the H_{13} recombination time scale, thus a constant power spectrum suppression traces $\alpha_d \propto (m_{\chi_3})^{-\frac{1}{2}}$ for a constant H_{13} binding energy, but they do not depend strongly on m_{χ_1}. The interesting regions for addressing the σ_8 problem are shown by the yellow bands.

- **Small scale structure:** We fix the ratio of the hyperfine splitting to the ground state energy as in Eq. (4.30). The mass of the intermediate DM flavor (χ_2 for the upper row of plots, and χ_1 for the lower row) is then determined at each point. This is indicated by the frame labels on the right-hand side of each plot. The preferred α_d interval for solving both the dwarf and cluster mass deficit problems from ref. [101] is indicated by the blue shaded bands.

- **Constraints from dark disc formation:** As explained in the previous section, the formation of a dark disc is possible in the red shaded region, which is therefore disfavored.

In summary, the overlap region between the yellow and blue bands that is outside of the red region gives the most preferred parameter space for addressing structure formation puzzles at different scales. This favors the ranges $\alpha_d \approx 0.02\text{-}0.04$, 20-45 GeV for the mass of the heaviest DM flavor, and the MeV scale for the mass of the lightest flavor. We reiterate that in this study we have taken a relatively simple approach to demonstrate that our model has the potential to solve the relevant structure formation problems; however a more careful study of the cosmological data and the Lyman-α constraints should be performed to fully establish this claim and determine the precise region in the parameter region where all conditions of interest are satisfied.
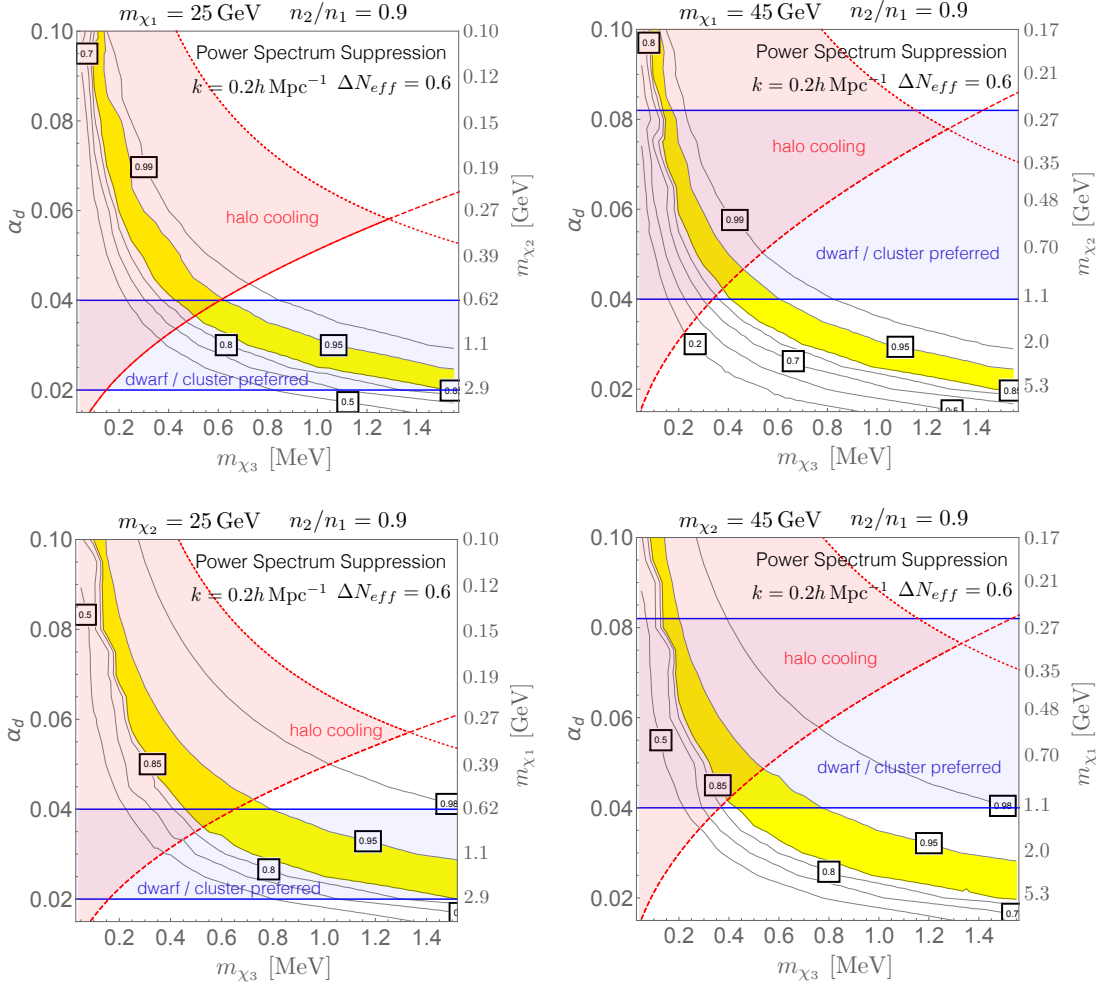
Figure 4.6: The combination of our results, for a few representative parameter choices. Plots on the left (right) column have the mass of the heaviest DM flavor at 25 (45) GeV. n_2/n_1 is chosen to be 0.9 in all plots. In the upper row, χ_1 is the heaviest flavor, so its mass is fixed, while the mass of χ_2 varies according to the $E_{hf}/E_0 = 10^{-4}$ benchmark we have adopted (as indicated by the frame labels on the right-hand side of the plots). In the lower row, the roles of χ_1 and χ_2 are reversed. As a function of m_{χ_3} and α_d, between the yellow shaded contours the matter power is suppressed by 5-15%, which may explain the smaller σ_8 value from late-time measurements compared to the value obtained by Planck. The blue-shaded bands show the preferred α_d interval where the mass deficit problem from dwarf galaxies to clusters is addressed. The red shaded region is disfavored by dark disc constraints as it allows for efficient cooling of the DM during halo formation. The preferred parameter space is therefore given by the overlap of the yellow and blue bands that is outside of the red shaded region.

4.3   Conclusions

We have explored the cosmological and astrophysical implications of a model of Secretly Asymmetric Dark Matter, where flavor-by-flavor asymmetries are generated in the dark sector through the decay of heavy right-handed neutrinos, despite an exact gauged dark $U(1)$. As a result, the total dark charge of the universe is always zero, and the DM flavors have opposite signs of the asymmetry, making it possible for bound states to form. When the heaviest dark matter flavor has a mass of $\mathcal{O}(10)$ GeV, the intermediate flavor has a mass of $\mathcal{O}(0.1-1)$ GeV, and the lightest flavor has a mass of $\mathcal{O}(1)$ MeV, with an $\alpha_d \sim 10^{-2}$ and $n_3/n_1 \sim 0.1$, this model can address several outstanding puzzles. In particular, the dark photon as an additional degree of freedom helps resolve the discrepancy between CMB-based and low redshift measurements of H_0, the resulting dark acoustic oscillations help address the σ_8 problem, and scattering between the bound states H_{12} after halo formation, with an inelastic component through the hyperfine transition, helps resolve issues at the cluster and dwarf galaxy scales. The model is consistent with constraints from short distance physics such as bounds on millicharged DM.

We want to emphasize that while we have chosen the DM to have three flavors for simplicity, the SADM mechanism works for a larger number of flavors as well, resulting in potentially even richer dynamical phenomena due to the increased number of relevant energy scales. We leave the exploration of this possibility to future work. Note also that as experimental sensitivity to millicharged DM increases, especially as the mass threshold of direct detection experiments is lowered, the parameter region of interest to this study should become testable in the not too distant future. Also, if the mass of the mediator ϕ is smaller than the benchmark value taken in equation 4.11, the lifetime of the heavier DM flavors can enter the regime where decaying DM signatures might become observable.

Appendix A: Lepton-flavored asymmetric dark matter

Since we wish to compare the parameter space consistent with direct detection bounds when the DM is asymmetric with the usual thermal relic case, we need to calculate the relic abundance in our model when no asymmetry is generated at high scales. Here we list the results of this calculation, for the scalar and fermion DM cases.

A.1 Relic density calculations: scalar dark matter

The coupling to the Higgs gives rise to the following annihilation channels, with their respective cross sections:

- $\chi\chi \to f\bar{f}$:

$$\sigma v_{\text{rel}} = \frac{1}{4\pi} N_C^f \lambda_{\chi h}^2 \beta_f^3 m_f^2 \frac{1}{(s - m_h^2)^2 + m_h^2 \Gamma_h^2}, \tag{A.1}$$

where $\beta_i = \sqrt{1 - 4m_i^2/s}$.

- $\chi\chi \to VV$:

$$\begin{aligned}
\sigma v_{\text{rel}} &= \frac{1}{1 + \delta_{VZ}} \frac{1}{8\pi} \lambda_{\chi h}^2 \beta_V \frac{s}{(s - m_h^2)^2 + m_h^2 \Gamma_h^2} \times \\
&\quad \left(1 - 4\frac{m_V^2}{s} + 12\frac{m_V^4}{s^2}\right),
\end{aligned} \tag{A.2}$$

where δ_{VZ} is 1 for the Z boson and 0 for the W boson.

- $\chi\chi \to hh$:

$$\begin{aligned}
\sigma v_{\text{rel}} &= \frac{\lambda_{\chi h}^2 \beta_h}{16\pi s} \left[\left(\frac{s + 2m_h^2}{s - m_h^2}\right)^2 + \frac{2\lambda_{\chi h}^2 v^4}{(m_\chi^2 - t_-)(m_\chi^2 - t_+)} \right. \\
&\quad \left. + 4\lambda_{\chi h} \frac{v^2}{s\beta_\chi \beta_h} \left(\frac{s + 2m_h^2}{s - m_h^2} - \frac{\lambda_{\chi h} v^2}{s - 2m_h^2}\right) \log\left|\frac{m_\chi^2 - t_+}{m_\chi^2 - t_-}\right| \right],
\end{aligned} \tag{A.3}$$

where $t_\pm = m_\chi^2 + m_h^2 - \frac{1}{2}s(1 \mp \beta_\chi \beta_h)$.

The FDM coupling of Eq. (2.1) gives rise to the annihilation channel $\chi^*\chi \to \ell^+\ell^-$. The cross section can be written as

$$\sigma v_{\text{rel}} = a + b v^2, \tag{A.4}$$

where

$$a = \frac{\lambda_\phi^4}{16\pi} \frac{m_f^2}{(m_\phi^2 + m_\chi^2 - m_f^2)^2} \left(1 - \frac{m_f^2}{m_\chi^2}\right)^{\frac{3}{2}}, \tag{A.5}$$

$$b = \frac{\lambda_\phi^4}{48\pi} \frac{m_\chi^2}{(m_\phi^2 + m_\chi^2)^2}. \tag{A.6}$$

Note that the s-wave contribution is chirality-suppressed.

A.2 Relic density calculations: fermion dark matter

The coupling to the Higgs gives rise to the following annihilation channels, with their respective cross sections:

- $\chi\chi \to f\bar{f}$:

$$\sigma v_{\text{rel}} = \frac{1}{8\pi} N_C^f \frac{\lambda_{\chi h}^2 m_f^2}{v^2} \beta_\chi^2 \beta_f^3 \frac{s}{(s - m_h^2)^2 + m_h^2 \Gamma_h^2}. \tag{A.7}$$

- $\chi\chi \to VV$:

$$\sigma v_{\text{rel}} = \frac{1}{1 + \delta_{VZ}} \frac{1}{16\pi} \frac{\lambda_{\chi h}^2}{v^2} \beta_\chi^2 \beta_V \frac{s^2}{(s - m_h^2)^2 + m_h^2 \Gamma_h^2} \times$$
$$\left(1 - 4\frac{m_V^2}{s} + 12\frac{m_V^4}{s^2}\right). \tag{A.8}$$

- $\chi\chi \to hh$:

$$\sigma v_{\text{rel}} = \frac{\lambda_{\chi h}^2 \beta_h \beta_\chi^2}{32\pi v^2} \left[\left(\frac{s + 2m_h^2}{s - m_h^2} \right)^2 + \frac{8\lambda_{\chi h} m_\chi v \, (s + 2m_h^2)}{\beta_\chi^2 s \, (s - m_h^2)} \right.$$
$$- \frac{2\lambda_{\chi h}^2 v^2 \left(3m_h^4 - 16m_h^2 m_\chi^2 + 2m_\chi^2 \left(s + 8m_\chi^2 \right) \right)}{\beta_\chi^2 s \left(m_h^4 - 4m_h^2 m_\chi^2 + m_\chi^2 s \right)}$$
$$+ \frac{2v\lambda_{\chi h}}{\beta_h \beta_\chi^3 s^2} \left(\frac{v\lambda_{\chi h} \left(6m_h^4 - 4m_h^2 \left(s + 4m_\chi^2 \right) - 32m_\chi^4 + 16m_\chi^2 s + s^2 \right)}{s - 2m_h^2} \right.$$
$$\left. \left. - \frac{2m_\chi \left(s + 2m_h^2 \right) \left(2m_h^2 - 8m_\chi^2 + s \right)}{m_h^2 - s} \right) \log \left| \frac{m_\chi^2 - t_+}{m_\chi^2 - t_-} \right| \right]. \tag{A.9}$$

The FDM coupling of Eq. (2.2) gives rise to the annihilation channel $\bar{\chi}\chi \to \ell^+\ell^-$. Unlike the scalar DM case, here the cross section is dominated by the s-wave:

$$\sigma v_{\text{rel}} = \frac{\lambda_\phi^4}{32\pi} \frac{m_\chi^2}{(m_\chi^2 + m_\phi^2 - m_f^2)^2} \sqrt{1 - \frac{m_f^2}{m_\chi^2}}. \tag{A.10}$$

A.3 The effective DM-photon coupling: scalar dark matter

The DM-photon interaction induced at one-loop has the form

$$\mathcal{L}_{\text{eff}} = i b_\chi \partial_\mu \chi^* \partial_\nu \chi F^{\mu\nu} \tag{A.11}$$

where

$$b_\chi = -\frac{e\lambda^2}{16\pi^2} \int_0^1 dy \left[\frac{y^3(\Delta_0(6 - 4y) + y(m_\chi^2(1 - y)^2 + m_\phi^2))}{3\Delta_0^2} \right.$$
$$\left. - (m_\phi^2 \leftrightarrow m_\ell^2) \right], \tag{A.12}$$

and

$$\Delta_0 \equiv m_\phi^2 y + (1 - y)m_\ell^2 - y(1 - y)m_\chi^2. \tag{A.13}$$

In the limit $m_\chi \ll m_\phi$ and $m_\ell \ll m_\phi$, b_χ is given to leading order by

$$b_\chi = \frac{\lambda^2 e}{16\pi^2 m_\phi^2} \left(1 - \frac{4}{3} \log \left(\frac{m_\ell}{m_\phi} \right) \right). \tag{A.14}$$

A.4 The effective DM-photon coupling: fermion dark matter

The DM-photon interaction induced at one-loop has the form

$$\mathcal{L}_{\text{eff}} = b_\chi \bar{\chi}\gamma_\nu\chi\partial_\mu F^{\mu\nu} + \mu_\chi \bar{\chi}i\sigma_{\mu\nu}\chi F^{\mu\nu}, \qquad (A.15)$$

where

$$\mu_\chi = -\frac{ie\lambda^2}{64\pi^2}\int_0^1 dy\; 2m_\chi\frac{y(1-y)}{\Delta_0}, \qquad (A.16)$$

$$b_\chi = -\frac{ie\lambda^2}{64\pi^2}\int_0^1 dy\; \frac{1}{6}y\left[(y^2-3y)\left(\frac{1}{\Delta_0}-\frac{1}{\Delta_0'}\right) + (y^2-6y+3)\frac{1}{\Delta_0}\right.$$
$$\left. +(y^2-3y)\frac{m_\ell^2}{\Delta_0^2}\right], \qquad (A.17)$$

and

$$\Delta_0 = ym_\ell^2 + (1-y)m_\phi^2 - y(1-y)m_\chi^2, \qquad (A.18)$$

$$\Delta_0' = ym_\phi^2 + (1-y)m_\ell^2 - y(1-y)m_\chi^2. \qquad (A.19)$$

In the limit $m_\chi \ll m_\phi$ and $m_\ell \ll m_\phi$, μ_χ and b_χ are given to leading order by

$$\mu_\chi = -\frac{e\lambda^2 m_\chi}{64\pi^2 m_\phi^2}, \qquad (A.20)$$

$$b_\chi = -\frac{i\lambda^2 e}{64\pi^2 m_\phi^2}\left(1+\frac{2}{3}\log\frac{m_\ell^2}{m_\phi^2}\right). \qquad (A.21)$$

A.5 Including the magnetic dipole interaction in direct detection

In this appendix we report the calculation details related to obtaining the direct detection bound for the fermion DM case when the dipole interaction is taken into account. The one-loop induced effective Lagrangian at the nucleon level is

$$\mathcal{L}_{\text{eff}} = c_\gamma^N \bar{\chi}\gamma^\mu\chi\overline{N}\gamma_\mu N + c_Q^N \bar{\chi}i\sigma^{\alpha\mu}\frac{k_\alpha}{k^2}\chi\overline{N}K_\mu N + c_\mu^N \bar{\chi}i\sigma^{\alpha\mu}\frac{k_\alpha}{k^2}\chi\overline{N}i\sigma^{\beta\mu}k_\beta N \text{(A.22)}$$

where

$$c_\gamma^N = eQ_N b_\chi, \quad c_Q^N = eQ_N\mu_\chi, \quad c_\mu^N = -e\tilde{\mu}_N\mu_\chi. \qquad (A.23)$$

Due to the nontrivial momentum dependence of these operators, we cannot directly use the elastic cross section bounds reported by the direct detection experiments. We thus proceed to calculate the differential rate and the event rate based on the parameters of the direct detection experiment and on the local DM velocity distribution. The differential scattering rate is given by

$$\frac{d\mathcal{R}}{dE_R} = N_T \frac{\rho_\chi}{m_\chi} \int_{v_{\min}} v f(\mathbf{v}) \frac{d\sigma}{dE_R} d^3\mathbf{v}, \tag{A.24}$$

where $f(\mathbf{v})$ is the local dark matter velocity distribution, ρ_χ is the local DM density (taken to be 0.3 GeV/cm^3), and N_T denotes the number of target nuclei per unit mass of the detector.

Let us start with the differential scattering cross section $\frac{d\sigma}{dE_R}$. In the nonrelativistic limit, the leading contributions [49, 50] to the relativistic nucleon-level operators are

$$\langle \chi, N \left| \overline{\chi}\gamma^\mu \chi \overline{N}\gamma_\mu N \right| \chi, N \rangle = 4m_\chi m_N, \tag{A.25}$$

$$\langle \chi, N \left| \overline{\chi} i\sigma^{\alpha\mu}\frac{k_\alpha}{k^2}\chi \overline{N} K_\mu N \right| \chi, N \rangle = 4m_N^2 + 16i\frac{m_N^3 m_\chi}{k^2}\vec{v}^\perp \cdot \left(\frac{\vec{k}}{m_N} \times \vec{S}_\chi \right), \tag{A.26}$$

$$\langle \chi, N \left| \overline{\chi} i\sigma^{\alpha\mu}\frac{k_\alpha}{k^2}\chi \overline{N} i\sigma^{\beta\mu}k_\beta N \right| \chi, N \rangle = 16m_\chi m_N \frac{m_N^2}{k^2} \left(\frac{\vec{k}}{m_N} \times \vec{S}_\chi \right) \cdot \left(\frac{\vec{k}}{m_N} \times \vec{S}_N \right). \tag{A.27}$$

At the nuclear level, taking the nuclear responses into account, and averaging over spins, we get

$$\frac{1}{2(2J+1)} \frac{1}{(4m_\chi m_T)^2} \sum_{\text{spin}} |\mathcal{M}|^2_{\text{nuclear}} = e^2 b_\chi^2 \tilde{W}_M^{(p,p)}$$

$$+ e^2 \mu_\chi^2 \left(\frac{\vec{v}^2}{\vec{k}^2} - \frac{1}{4\mu_{\chi T}^2} + \frac{1}{4m_\chi^2} \right) \tilde{W}_M^{(p,p)}$$

$$+ \frac{e^2 \mu_\chi^2}{m_N^2} \left[\tilde{W}_\Delta^{(p,p)} - \tilde{\mu}_n \tilde{W}_{\Delta\Sigma'}^{(p,n)} - \tilde{\mu}_p \tilde{W}_{\Delta\Sigma'}^{(p,p)} \right.$$

$$\left. + \frac{1}{4} \left(\tilde{\mu}_p^2 \tilde{W}_{\Sigma'}^{(p,p)} + 2\tilde{\mu}_n\tilde{\mu}_p \tilde{W}_{\Sigma'}^{(p,n)} + \tilde{\mu}_n^2 \tilde{W}_{\Sigma'}^{(n,n)} \right) \right], \tag{A.28}$$

where $\tilde{W}_i^{(N,N)}$ are nuclear response functions with nuclear spin average factor $\frac{1}{2J+1}$ included, defined in Refs. [49, 50]. We use the shell model to write the magnetic moment of a nucleus as

$$\tilde{\mu}_T = 2\tilde{\mu}_p\langle S_p \rangle + 2\tilde{\mu}_n\langle S_n \rangle + \langle L_p \rangle. \tag{A.29}$$

In the $q^2 \to 0$ limit, the term in square brackets in Eq. (A.28) goes to $\frac{J+1}{6J}\tilde{\mu}_T^2$, while $\tilde{W}_M^{(p,p)}$ becomes Z^2. Eq. (A.28) thus simplifies to

$$\frac{1}{2(2J+1)}\frac{1}{(4m_\chi m_T)^2} \quad \sum_{\text{spin}}|\mathcal{M}|^2_{\text{nuclear}} = e^2\mu_\chi^2\left[\frac{\vec{v}^2}{\vec{k}^2} - \frac{1}{4}\left(\frac{2}{m_T m_\chi} + \frac{1}{m_T^2}\right)\right] \times$$
$$Z^2 F^2(A;k^2) + e^2\mu_\chi^2\frac{J+1}{3J}\frac{\tilde{\mu}_T^2}{2m_N^2}, \tag{A.30}$$

where $F(A;k^2)$ is the Helm form factor. With this, the differential cross section becomes (consistent with Refs. [51, 52])

$$\frac{\mathrm{d}\sigma}{\mathrm{dE_R}} = \frac{m_T}{2\pi v^2}\left\{e^2 b_\chi^2 Z^2 F^2(A;k^2) + e^2\mu_\chi^2\left[\frac{\vec{v}^2}{\vec{k}^2} - \frac{1}{4}\left(\frac{2}{m_T m_\chi} + \frac{1}{m_T^2}\right)\right]Z^2 F^2(A;k^2)\right.$$
$$\left. + e^2\mu_\chi^2\frac{J+1}{3J}\frac{\tilde{\mu}_T^2}{2m_N^2}\right\}. \tag{A.31}$$

We next turn our attention to modeling detector effects of the direct detection experiment. In particular, we have to take into account that the measured energy is only part of the true recoil energy E_R, that the experiment has a finite energy resolution and that the analysis involves cuts, the efficiencies of which will enter the calculation of the differential rate.

The LUX experiment uses the direct scintillation (S1) and ionization signals (S2) to reject backgrounds. Both the S1 and S2 signals are detected by arrays of photomultipliers (PMTs), and measured in numbers of photoelectrons (PE). The expected number of photoelectrons [53, 43] is

$$\nu(E_R) = E_R \times \mathcal{L}_{eff} \times L_y S_{\text{nr}}/S_{\text{ee}}. \tag{A.32}$$

In using this formula, we take the values for the scintillation efficiency $\mathcal{L}_{eff}$ and energy dependent absolute light yield $L_y S_{\text{nr}}/S_{\text{ee}}$ (with scintillation quenching factors for electron and nuclear recoils included) from page 25 of the slides at `http://luxdarkmatter.org/talks/20131030_LUX_First_Results.pdf`.

The smearing function has a mean n and variance $\sqrt{n}\sigma_{\text{PMT}}$ with $\sigma_{\text{PMT}} = 0.37$ PE. Since the analysis uses the lower half of the signal band, the cut efficiency is taken to be 50% [43]. The number of signal events thus becomes

$$N = \text{Ex} \times \int_{S1_{\text{low}}}^{S1_{up}} \mathrm{d}S1\ \mathcal{E}(S1)\sum_{n=1}^{\infty}\text{Gauss}(S1|n,\sqrt{n}\sigma_{\text{PMT}}) \times$$
$$\int_0^\infty \mathrm{d}E_R\ \text{Poisson}(n|\nu(E_R))\frac{\mathrm{d}\mathcal{R}}{\mathrm{d}E_R}. \tag{A.33}$$

where the $S1$ integration range is $2\,\mathrm{PE} \leq S_1 \leq 30\,\mathrm{PE}$, and Ex denotes the experimental exposure, taken to be 85.3×118 kg-days.

Putting everything together, we calculate the probability for the signal plus background to have given rise to no more than one event (as was observed by LUX). This is given as

$$\mathcal{L} = \sum_{k=0}^{1} \int \mathrm{d}\mu_B \mathrm{Gauss}(\mu_B|N_B, \sigma_B)\mathrm{Poisson}(k|N_B + N_S), \qquad (\mathrm{A.34})$$

where N_S is the expected number of the signal events, N_B is the expected number of background events and σ_B is its variance. We take the latter two parameters to be 0.64 ± 0.16. We then use $\mathcal{L}$ to set to bound on N_S at 90% confidence level, which can then be translated to a bound in terms of the model parameters.

Bibliography

[1] Y. Nir, CERN-2015-001, pp.123-156 doi:10.5170/CERN-2015-001.123 [arXiv:1605.00433 [hep-ph]]. 2

[2] M. Tanabashi *et al.* (Particle Data Group), Phys. Rev. D **98**, 030001 (2018) doi:10.1103/PhysRevD.98.030001 3

[3] A. D. Sakharov, Pisma Zh. Eksp. Teor. Fiz. **5**, 32 (1967) [JETP Lett. **5**, 24 (1967)] [Sov. Phys. Usp. **34**, no. 5, 392 (1991)] [Usp. Fiz. Nauk **161**, no. 5, 61 (1991)]. doi:10.1070/PU1991v034n05ABEH002497 3

[4] A. Hamze, C. Kilic, J. Koeller, C. Trendafilova and J. H. Yu, Phys. Rev. D **91**, no. 3, 035009 (2015) doi:10.1103/PhysRevD.91.035009 [arXiv:1410.3030 [hep-ph]]. 8, 29

[5] D. Tucker-Smith and N. Weiner, Phys. Rev. D **64**, 043502 (2001) doi:10.1103/PhysRevD.64.043502 [hep-ph/0101138]. 8

[6] D. Tucker-Smith and N. Weiner, Phys. Rev. D **72**, 063509 (2005) doi:10.1103/PhysRevD.72.063509 [hep-ph/0402065]. 8

[7] S. Chang, G. D. Kribs, D. Tucker-Smith and N. Weiner, Phys. Rev. D **79**, 043513 (2009) doi:10.1103/PhysRevD.79.043513 [arXiv:0807.2250 [hep-ph]]. 8

[8] J. L. Feng, J. Kumar, D. Marfatia and D. Sanford, Phys. Lett. B **703**, 124 (2011) doi:10.1016/j.physletb.2011.07.083 [arXiv:1102.4331 [hep-ph]]. 8

[9] S. Chang, J. Liu, A. Pierce, N. Weiner and I. Yavin, JCAP **1008**, 018 (2010) doi:10.1088/1475-7516/2010/08/018 [arXiv:1004.0697 [hep-ph]]. 8

[10] P. J. Fox, J. Liu, D. Tucker-Smith and N. Weiner, Phys. Rev. D **84**, 115006 (2011) doi:10.1103/PhysRevD.84.115006 [arXiv:1104.4127 [hep-ph]]. 8

[11] X. Gao, Z. Kang and T. Li, JCAP **1301**, 021 (2013) doi:10.1088/1475-7516/2013/01/021 [arXiv:1107.3529 [hep-ph]]. 8

[12] E. Del Nobile, C. Kouvaris, F. Sannino and J. Virkajarvi, Mod. Phys. Lett. A **27**, 1250108 (2012) doi:10.1142/S0217732312501088 [arXiv:1111.1902 [hep-ph]]. 8

[13] E. Del Nobile, C. Kouvaris and F. Sannino, Phys. Rev. D **84**, 027301 (2011) doi:10.1103/PhysRevD.84.027301 [arXiv:1105.5431 [hep-ph]]. 8

[14] M. T. Frandsen, F. Kahlhoefer, S. Sarkar and K. Schmidt-Hoberg, JHEP **1109**, 128 (2011) doi:10.1007/JHEP09(2011)128 [arXiv:1107.2118 [hep-ph]]. 8

[15] V. Cirigliano, M. L. Graesser, G. Ovanesyan and I. M. Shoemaker, Phys. Lett. B **739**, 293 (2014) doi:10.1016/j.physletb.2014.10.058 [arXiv:1311.5886 [hep-ph]]. 8

[16] N. Okada and O. Seto, Phys. Rev. D **88**, 063506 (2013) doi:10.1103/PhysRevD.88.063506 [arXiv:1304.6791 [hep-ph]]. 8

[17] G. Blanger, A. Goudelis, J. C. Park and A. Pukhov, JCAP **1402**, 020 (2014) doi:10.1088/1475-7516/2014/02/020 [arXiv:1311.0022 [hep-ph]]. 8

[18] K. Hamaguchi, S. P. Liew, T. Moroi and Y. Yamamoto, JHEP **1405**, 086 (2014) doi:10.1007/JHEP05(2014)086 [arXiv:1403.0324 [hep-ph]]. 8

[19] C. R. Chen, Y. K. Chu and H. C. Tsai, Phys. Lett. B **741**, 205 (2015) doi:10.1016/j.physletb.2014.12.043 [arXiv:1410.0918 [hep-ph]]. 8

[20] J. Kile and A. Soni, Phys. Rev. D **84**, 035016 (2011) doi:10.1103/PhysRevD.84.035016 [arXiv:1104.5239 [hep-ph]]. 8

[21] B. Batell, J. Pradler and M. Spannowsky, JHEP **1108**, 038 (2011) doi:10.1007/JHEP08(2011)038 [arXiv:1105.1781 [hep-ph]]. 8, 29, 39

[22] J. F. Kamenik and J. Zupan, Phys. Rev. D **84**, 111502 (2011) doi:10.1103/PhysRevD.84.111502 [arXiv:1107.0623 [hep-ph]]. 8

[23] P. Agrawal, S. Blanchet, Z. Chacko and C. Kilic, Phys. Rev. D **86**, 055002 (2012) doi:10.1103/PhysRevD.86.055002 [arXiv:1109.3516 [hep-ph]]. 8, 10, 13, 16, 27, 29, 39

[24] A. Kumar and S. Tulin, Phys. Rev. D **87**, no. 9, 095006 (2013) doi:10.1103/PhysRevD.87.095006 [arXiv:1303.0332 [hep-ph]]. 8, 29

[25] S. Chang, R. Edezhath, J. Hutchinson and M. Luty, Phys. Rev. D **89**, no. 1, 015011 (2014) doi:10.1103/PhysRevD.89.015011 [arXiv:1307.8120 [hep-ph]]. 8

[26] Y. Bai and J. Berger, JHEP **1311**, 171 (2013) doi:10.1007/JHEP11(2013)171 [arXiv:1308.0612 [hep-ph]]. 8

[27] B. Batell, T. Lin and L. T. Wang, JHEP **1401**, 075 (2014) doi:10.1007/JHEP01(2014)075 [arXiv:1309.4462 [hep-ph]]. 8, 29

[28] P. Agrawal, M. Blanke and K. Gemmler, JHEP **1410**, 072 (2014) doi:10.1007/JHEP10(2014)072 [arXiv:1405.6709 [hep-ph]]. 8, 29, 39

[29] P. Agrawal, B. Batell, D. Hooper and T. Lin, Phys. Rev. D **90**, no. 6, 063512 (2014) doi:10.1103/PhysRevD.90.063512 [arXiv:1404.1373 [hep-ph]]. 8, 29

[30] P. Agrawal, Z. Chacko and C. B. Verhaaren, JHEP **1408**, 147 (2014) doi:10.1007/JHEP08(2014)147 [arXiv:1402.7369 [hep-ph]]. 8

[31] S. Nussinov, Phys. Lett. B **165**, no. 1, 55 (1985) doi:10.1016/0370-2693(85)90689-6 9, 28

[32] D. B. Kaplan, Phys. Rev. Lett. **68**, no. 6, 741 (1992) doi:10.1103/PhysRevLett.68.741 9, 28

[33] S. M. Barr, R. S. Chivukula and E. Farhi, Phys. Lett. B **241**, no. 3, 387 (1990) doi:10.1016/0370-2693(90)91661-T 9, 28

[34] D. E. Kaplan, M. A. Luty and K. M. Zurek, Phys. Rev. D **79**, 115016 (2009) doi:10.1103/PhysRevD.79.115016 [arXiv:0901.4117 [hep-ph]]. 9, 28

[35] A. Falkowski, J. T. Ruderman and T. Volansky, JHEP **1105**, 106 (2011) doi:10.1007/JHEP05(2011)106 [arXiv:1101.4936 [hep-ph]]. 9, 28

[36] K. M. Zurek, Phys. Rept. **537**, 91 (2014) doi:10.1016/j.physrep.2013.12.001 [arXiv:1308.0338 [hep-ph]]. 9, 28

[37] K. Petraki and R. R. Volkas, Int. J. Mod. Phys. A **28**, 1330028 (2013) doi:10.1142/S0217751X13300287 [arXiv:1305.4939 [hep-ph]]. 9, 28

[38] M. Fukugita and T. Yanagida, Phys. Lett. B **174**, 45 (1986). doi:10.1016/0370-2693(86)91126-3 9, 29, 38

[39] W. Buchmuller, R. D. Peccei and T. Yanagida, Ann. Rev. Nucl. Part. Sci. **55**, 311 (2005) doi:10.1146/annurev.nucl.55.090704.151558 [hep-ph/0502169]. 9, 12

[40] M. C. Chen, hep-ph/0703087 [HEP-PH]. 9, 12

[41] G. D'Ambrosio, G. F. Giudice, G. Isidori and A. Strumia, Nucl. Phys. B **645**, 155 (2002) doi:10.1016/S0550-3213(02)00836-2 [hep-ph/0207036]. 10

[42] G. Belanger, F. Boudjema, A. Pukhov and A. Semenov, Comput. Phys. Commun. **185**, 960 (2014) doi:10.1016/j.cpc.2013.10.016 [arXiv:1305.0237 [hep-ph]]. 15

[43] D. S. Akerib *et al.* [LUX Collaboration], Phys. Rev. Lett. **112**, 091303 (2014) doi:10.1103/PhysRevLett.112.091303 [arXiv:1310.8214 [astro-ph.CO]]. 17, 19, 66

[44] R. Agnese *et al.* [CDMS Collaboration], Phys. Rev. Lett. **111**, no. 25, 251301 (2013) doi:10.1103/PhysRevLett.111.251301 [arXiv:1304.4279 [hep-ex]]. 19

[45] R. Agnese *et al.* [SuperCDMS Collaboration], Phys. Rev. Lett. **112**, no. 4, 041302 (2014) doi:10.1103/PhysRevLett.112.041302 [arXiv:1309.3259 [physics.ins-det]]. 19

[46] G. Angloher *et al.* [CRESST-II Collaboration], Eur. Phys. J. C **74**, no. 12, 3184 (2014) doi:10.1140/epjc/s10052-014-3184-9 [arXiv:1407.3146 [astro-ph.CO]]. 19

[47] S. Chatrchyan *et al.* [CMS Collaboration], Eur. Phys. J. C **74**, 2980 (2014) doi:10.1140/epjc/s10052-014-2980-6 [arXiv:1404.1344 [hep-ex]]. 19

[48] G. Aad *et al.* [ATLAS Collaboration], Phys. Rev. Lett. **112**, 201802 (2014) doi:10.1103/PhysRevLett.112.201802 [arXiv:1402.3244 [hep-ex]]. 19

[49] A. L. Fitzpatrick, W. Haxton, E. Katz, N. Lubbers and Y. Xu, JCAP **1302**, 004 (2013) doi:10.1088/1475-7516/2013/02/004 [arXiv:1203.3542 [hep-ph]]. 65

[50] M. I. Gresham and K. M. Zurek, Phys. Rev. D **89**, no. 12, 123521 (2014) doi:10.1103/PhysRevD.89.123521 [arXiv:1401.3739 [hep-ph]]. 65

[51] V. Barger, W. Y. Keung and D. Marfatia, Phys. Lett. B **696**, 74 (2011) doi:10.1016/j.physletb.2010.12.008 [arXiv:1007.4345 [hep-ph]]. 66

[52] M. I. Gresham and K. M. Zurek, Phys. Rev. D **89**, no. 1, 016017 (2014) doi:10.1103/PhysRevD.89.016017 [arXiv:1311.2082 [hep-ph]]. 66

[53] E. Aprile *et al.* [XENON100 Collaboration], Phys. Rev. Lett. **107**, 131302 (2011) doi:10.1103/PhysRevLett.107.131302 [arXiv:1104.2549 [astro-ph.CO]]. 66

[54] P. Agrawal, C. Kilic, S. Swaminathan and C. Trendafilova, Phys. Rev. D **95**, no. 1, 015031 (2017) doi:10.1103/PhysRevD.95.015031 [arXiv:1608.04745 [hep-ph]]. 28, 38, 39

[55] G. B. Gelmini, L. J. Hall and M. J. Lin, Nucl. Phys. B **281**, 726 (1987(doi:10.1016/0550-3213(87)90424-X 28

[56] S. M. Barr, Phys. Rev. D **44**, 3062 (1991) doi:10.1103/PhysRevD.44.3062 28

[57] E. Hardy, R. Lasenby and J. Unwin, JHEP **1407**, 049 (2014) doi:10.1007/JHEP07(2014)049 [arXiv:1402.4500 [hep-ph]]. 28

[58] M. R. Buckley and S. Profumo, Phys. Rev. Lett. **108**, 011301 (2012) doi:10.1103/PhysRevLett.108.011301 [arXiv:1109.2164 [hep-ph]]. 28

[59] M. Cirelli, P. Panci, G. Servant and G. Zaharijas, JCAP **1203**, 015 (2012) doi:10.1088/1475-7516/2012/03/015 [arXiv:1110.3809 [hep-ph]]. 28

[60] S. Tulin, H. B. Yu and K. M. Zurek, JCAP **1205**, 013 (2012) doi:10.1088/1475-7516/2012/05/013 [arXiv:1202.0283 [hep-ph]]. 28

[61] N. Okada and O. Seto, Phys. Rev. D **86**, 063525 (2012) doi:10.1103/PhysRevD.86.063525 [arXiv:1205.2844 [hep-ph]]. 28

[62] S. L. Chen and Z. Kang, Phys. Lett. B **761**, 296 (2016) doi:10.1016/j.physletb.2016.08.051 [arXiv:1512.08780 [hep-ph]]. 28

[63] J. March-Russell, C. McCabe and M. McCullough, JHEP **1003**, 108 (2010) doi:10.1007/JHEP03(2010)108 [arXiv:0911.4489 [hep-ph]]. 29, 39

[64] J. Kile, Mod. Phys. Lett. A **28**, 1330031 (2013) doi:10.1142/S0217732313300310 [arXiv:1308.0584 [hep-ph]]. 29, 39

[65] L. Lopez-Honorez and L. Merlo, Phys. Lett. B **722**, 135 (2013) doi:10.1016/j.physletb.2013.04.015 [arXiv:1303.1087 [hep-ph]]. 29

[66] C. J. Lee and J. Tandean, JHEP **1504**, 174 (2015) doi:10.1007/JHEP04(2015)174 [arXiv:1410.6803 [hep-ph]]. 29

[67] C. Kilic, M. D. Klimek and J. H. Yu, Phys. Rev. D **91**, no. 5, 054036 (2015) doi:10.1103/PhysRevD.91.054036 [arXiv:1501.02202 [hep-ph]]. 29

[68] F. Bishara, A. Greljo, J. F. Kamenik, E. Stamou and J. Zupan, JHEP **1512**, 130 (2015) doi:10.1007/JHEP12(2015)130 [arXiv:1505.03862 [hep-ph]]. 29

[69] B. Bhattacharya, D. London, J. M. Cline, A. Datta and G. Dupuis, Phys. Rev. D **92**, no. 11, 115012 (2015) doi:10.1103/PhysRevD.92.115012 [arXiv:1509.04271 [hep-ph]]. 29

[70] L. Calibbi, A. Crivellin and B. Zaldvar, Phys. Rev. D **92**, no. 1, 016004 (2015) doi:10.1103/PhysRevD.92.016004 [arXiv:1501.07268 [hep-ph]]. 29

[71] S. Baek and Z. F. Kang, JHEP **1603**, 106 (2016) doi:10.1007/JHEP03(2016)106 [arXiv:1510.00100 [hep-ph]]. 29

[72] M. C. Chen, J. Huang and V. Takhistov, JHEP **1602**, 060 (2016) doi:10.1007/JHEP02(2016)060 [arXiv:1510.04694 [hep-ph]]. 29, 39

[73] S. Davidson, E. Nardi and Y. Nir, Phys. Rept. **466**, 105 (2008) doi:10.1016/j.physrep.2008.06.002 [arXiv:0802.2962 [hep-ph]]. 29, 38, 40, 43

[74] C. S. Fong, E. Nardi and A. Riotto, Adv. High Energy Phys. **2012**, 158303 (2012) doi:10.1155/2012/158303 [arXiv:1301.3062 [hep-ph]]. 29, 38, 40

[75] P. A. R. Ade *et al.* [Planck Collaboration], Astron. Astrophys. **594**, A13 (2016) doi:10.1051/0004-6361/201525830 [arXiv:1502.01589 [astro-ph.CO]]. xi, 33, 35

[76] J. March-Russell, H. Murayama and A. Riotto, JHEP **9911**, 015 (1999) doi:10.1088/1126-6708/1999/11/015 [hep-ph/9908396]. 33

[77] P. Agrawal, Z. Chacko, C. Kilic and C. B. Verhaaren, JHEP **1508**, 072 (2015) doi:10.1007/JHEP08(2015)072 [arXiv:1503.03057 [hep-ph]]. 33

[78] B. Holdom, Phys. Lett. B **166**, 196 (1986) doi:10.1016/0370-2693(86)91377-8 34

[79] E. J. Chun, J. C. Park and S. Scopel, JHEP **1102**, 100 (2011) doi:10.1007/JHEP02(2011)100 [arXiv:1011.3300 [hep-ph]]. 34

[80] L. Accardo *et al.* (AMS), Phys. Rev. Lett. **113**, 121101 (2014) doi:10.1103/PhysRevLett.113.121101 xi, 34, 35

[81] M. Aguilar *et al.* (AMS), Phys. Rev. Lett. **113**, 121102 (2014) doi:10.1103/PhysRevLett.113.121102 xi, 34, 35

[82] M. Ackermann *et al.* [Fermi-LAT Collaboration], Phys. Rev. Lett. **115**, no. 23, 231301 (2015) doi:10.1103/PhysRevLett.115.231301 [arXiv:1503.02641 [astro-ph.HE]]. xi, 34, 35

[83] N. Arkani-Hamed, D. P. Finkbeiner, T. R. Slatyer and N. Weiner, Phys. Rev. D **79**, 015014 (2009) doi:10.1103/PhysRevD.79.015014 [arXiv:0810.0713 [hep-ph]]. 35

[84] T. R. Slatyer, Phys. Rev. D **93**, no. 2, 023527 (2016) doi:10.1103/PhysRevD.93.023527 [arXiv:1506.03811 [hep-ph]]. 35

[85] G. Elor, N. L. Rodd, T. R. Slatyer and W. Xue, JCAP **1606**, no. 06, 024 (2016) doi:10.1088/1475-7516/2016/06/024 [arXiv:1511.08787 [hep-ph]]. 35

[86] A. Manalaysay, **IDM2016**, `http://luxdarkmatter.org/LUX_dark_matter/ Talks_files/LUX_NewDarkMatterSearchResult_332LiveDays_IDM2016_ 160721.pdf` xi, 35, 36

[87] D. S. Akerib *et al.* [LUX Collaboration], Phys. Rev. Lett. **116**, no. 16, 161301 (2016) doi:10.1103/PhysRevLett.116.161301 [arXiv:1512.03506 [astro-ph.CO]]. xi, 35, 36

[88] R. Agnese *et al.* [SuperCDMS Collaboration], Phys. Rev. Lett. **116**, no. 7, 071301 (2016) doi:10.1103/PhysRevLett.116.071301 [arXiv:1509.02448 [astro-ph.CO]]. xi, 35, 36

[89] G. Angloher *et al.* [CRESST Collaboration], Eur. Phys. J. C **76**, no. 1, 25 (2016) doi:10.1140/epjc/s10052-016-3877-3 [arXiv:1509.01515 [astro-ph.CO]]. xi, 35, 36

[90] G. Steigman, B. Dasgupta and J. F. Beacom, Phys. Rev. D **86**, 023506 (2012) doi:10.1103/PhysRevD.86.023506 [arXiv:1204.3622 [hep-ph]]. xi, 35

[91] D. Curtin, R. Essig, S. Gori and J. Shelton, JHEP **1502**, 157 (2015) doi:10.1007/JHEP02(2015)157 [arXiv:1412.0018 [hep-ph]]. 36

[92] S. Alekhin *et al.*, Rept. Prog. Phys. **79**, no. 12, 124201 (2016) doi:10.1088/0034-4885/79/12/124201 [arXiv:1504.04855 [hep-ph]]. 36

[93] C. Dessert, C. Kilic, C. Trendafilova and Y. Tsai, Phys. Rev. D **100**, 015029 (2019) doi:10.1103/PhysRevD.100.015029 [arXiv:1811.05534 [hep-ph]]. 38

[94] J. H. Chang, R. Essig and S. D. McDermott, JHEP **1809**, 051 (2018) doi:10.1007/JHEP09(2018)051 [arXiv:1803.00993 [hep-ph]]. 38, 46

[95] Z. Chacko, Y. Cui, S. Hong, T. Okui and Y. Tsai, JHEP **1612**, 108 (2016) doi:10.1007/JHEP12(2016)108 [arXiv:1609.03569 [astro-ph.CO]]. 38

[96] M. A. Buen-Abad, M. Schmaltz, J. Lesgourgues and T. Brinckmann, JCAP **1801**, no. 01, 008 (2018) doi:10.1088/1475-7516/2018/01/008 [arXiv:1708.09406 [astro-ph.CO]]. 38

[97] M. Raveri, W. Hu, T. Hoffman and L. T. Wang, Phys. Rev. D **96**, no. 10, 103501 (2017) doi:10.1103/PhysRevD.96.103501 [arXiv:1709.04877 [astro-ph.CO]]. 38

[98] Z. Pan, M. Kaplinghat and L. Knox, Phys. Rev. D **97**, no. 10, 103531 (2018) doi:10.1103/PhysRevD.97.103531 [arXiv:1801.07348 [astro-ph.CO]]. 38

[99] F. Y. Cyr-Racine and K. Sigurdson, Phys. Rev. D **87**, no. 10, 103515 (2013) doi:10.1103/PhysRevD.87.103515 [arXiv:1209.5752 [astro-ph.CO]]. 38, 50

[100] F. Y. Cyr-Racine, R. de Putter, A. Raccanelli and K. Sigurdson, Phys. Rev. D **89**, no. 6, 063517 (2014) doi:10.1103/PhysRevD.89.063517 [arXiv:1310.3278 [astro-ph.CO]]. 55

[101] K. K. Boddy, M. Kaplinghat, A. Kwa and A. H. G. Peter, Phys. Rev. D **94**, no. 12, 123017 (2016) doi:10.1103/PhysRevD.94.123017 [arXiv:1609.03592 [hep-ph]]. 38, 56, 58

[102] Z. Chacko, D. Curtin, M. Geller and Y. Tsai, JHEP **1809**, 163 (2018) doi:10.1007/JHEP09(2018)163 [arXiv:1803.03263 [hep-ph]]. 38, 50

[103] J. L. Bernal, L. Verde and A. G. Riess, JCAP **1610**, no. 10, 019 (2016) doi:10.1088/1475-7516/2016/10/019 [arXiv:1607.05617 [astro-ph.CO]]. 38, 39

[104] M. Persic, P. Salucci and F. Stel, Mon. Not. Roy. Astron. Soc. **281**, 27 (1996) doi:10.1093/mnras/281.1.27, 10.1093/mnras/278.1.27 [astro-ph/9506004]. 38, 47

[105] Hildebrandt, H., Viola, M., Heymans, C., et al. 2017, MNRAS, 465, 1454 38, 47

[106] F. Köhlinger *et al.*, Mon. Not. Roy. Astron. Soc. **471**, no. 4, 4412 (2017) doi:10.1093/mnras/stx1820 [arXiv:1706.02892 [astro-ph.CO]]. 38, 47

[107] S. Joudaki *et al.*, Mon. Not. Roy. Astron. Soc. **474**, no. 4, 4894 (2018) doi:10.1093/mnras/stx2820 [arXiv:1707.06627 [astro-ph.CO]]. 38, 47

[108] M. A. Troxel *et al.* [DES Collaboration], Phys. Rev. D **98**, no. 4, 043528 (2018) doi:10.1103/PhysRevD.98.043528 [arXiv:1708.01538 [astro-ph.CO]]. 38, 47

[109] B. Moore, Nature **370**, 629 (1994). doi:10.1038/370629a0 38, 47

[110] Newman, A. B., Treu, T., Ellis, R. S., & Sand, D. J. (2013), APJ, 765, 25 38, 47

[111] J. M. Cline, Z. Liu and W. Xue, Phys. Rev. D **85**, 101302 (2012) doi:10.1103/PhysRevD.85.101302 [arXiv:1201.4858 [hep-ph]]. 39, 48

[112] R. Foot and S. Vagnozzi, Phys. Rev. D **91**, 023512 (2015) doi:10.1103/PhysRevD.91.023512 [arXiv:1409.7174 [hep-ph]]. 39

[113] M. A. Buen-Abad, G. Marques-Tavares and M. Schmaltz, Phys. Rev. D **92**, no. 2, 023531 (2015) doi:10.1103/PhysRevD.92.023531 [arXiv:1505.03542 [hep-ph]]. 39

[114] Z. Chacko, Y. Cui, S. Hong and T. Okui, Phys. Rev. D **92**, 055033 (2015) doi:10.1103/PhysRevD.92.055033 [arXiv:1505.04192 [hep-ph]]. 39

[115] J. Lesgourgues, G. Marques-Tavares and M. Schmaltz, JCAP **1602**, no. 02, 037 (2016) doi:10.1088/1475-7516/2016/02/037 [arXiv:1507.04351 [astro-ph.CO]]. 39

[116] P. Ko and Y. Tang, Phys. Lett. B **762**, 462 (2016) doi:10.1016/j.physletb.2016.10.001 [arXiv:1608.01083 [hep-ph]]. 39

[117] P. Ko and Y. Tang, Phys. Lett. B **768**, 12 (2017) doi:10.1016/j.physletb.2017.02.033 [arXiv:1609.02307 [hep-ph]]. 39

[118] V. Prilepina and Y. Tsai, JHEP **1709**, 033 (2017) doi:10.1007/JHEP09(2017)033 [arXiv:1611.05879 [hep-ph]]. 39

[119] P. Agrawal, F. Y. Cyr-Racine, L. Randall and J. Scholtz, JCAP **1708**, no. 08, 021 (2017) doi:10.1088/1475-7516/2017/08/021 [arXiv:1702.05482 [astro-ph.CO]]. 39

[120] I. Baldes, M. Cirelli, P. Panci, K. Petraki, F. Sala and M. Taoso, SciPost Phys. **4**, no. 6, 041 (2018) doi:10.21468/SciPostPhys.4.6.041 [arXiv:1712.07489 [hep-ph]]. 39

[121] P. Agrawal, Z. Chacko, E. C. F. S. Fortes and C. Kilic, Phys. Rev. D **93**, no. 10, 103510 (2016) doi:10.1103/PhysRevD.93.103510 [arXiv:1511.06293 [hep-ph]]. 39

[122] Goldberg, H., & Hall, L. J. 1986, Physics Letters B, 174, 151 39

[123] D. E. Kaplan, G. Z. Krnjaic, K. R. Rehermann and C. M. Wells, JCAP **1005**, 021 (2010) doi:10.1088/1475-7516/2010/05/021 [arXiv:0909.0753 [hep-ph]]. 39

[124] N. Aghanim *et al.* [Planck Collaboration], arXiv:1807.06209 [astro-ph.CO]. 39, 47, 48, 54

[125] A. G. Riess *et al.*, Astrophys. J. **861**, no. 2, 126 (2018) doi:10.3847/1538-4357/aac82e [arXiv:1804.10655 [astro-ph.CO]]. 39

[126] V. Bonvin *et al.*, Mon. Not. Roy. Astron. Soc. **465**, no. 4, 4914 (2017) doi:10.1093/mnras/stw3006 [arXiv:1607.01790 [astro-ph.CO]]. 39

[127] K. Kadota, T. Sekiguchi and H. Tashiro, arXiv:1602.04009 [astro-ph.CO]. 46

[128] A. G. Riess *et al.*, Astrophys. J. **826**, no. 1, 56 (2016) doi:10.3847/0004-637X/826/1/56 [arXiv:1604.01424 [astro-ph.CO]]. 47

[129] Riess, A. G., Casertano, S., Yuan, W., et al. 2018, APJ, 855, 136 48

[130] Spitzer, L., Jr., & Greenstein, J. L. 1951,APJ, 114, 407 50

[131] R. Cooke, M. Pettini, R. A. Jorgenson, M. T. Murphy and C. C. Steidel, Astrophys. J. **781**, no. 1, 31 (2014) doi:10.1088/0004-637X/781/1/31 [arXiv:1308.3240 [astro-ph.CO]]. 48

[132] J. M. Cline, Z. Liu, G. Moore and W. Xue, Phys. Rev. D **89**, no. 4, 043514 (2014) doi:10.1103/PhysRevD.89.043514 [arXiv:1311.6468 [hep-ph]].

[133] C. P. Ma and E. Bertschinger, Astrophys. J. **455**, 7 (1995) doi:10.1086/176550 [astro-ph/9506072]. 52, 53

[134] M. R. Buckley, J. Zavala, F. Y. Cyr-Racine, K. Sigurdson and M. Vogelsberger, Phys. Rev. D **90**, no. 4, 043524 (2014) doi:10.1103/PhysRevD.90.043524 [arXiv:1405.2075 [astro-ph.CO]]. 54

[135] S. Bose, M. Vogelsberger, J. Zavala, C. Pfrommer, F. Y. Cyr-Racine, S. Bohr and T. Bringmann, arXiv:1811.10630 [astro-ph.CO]. 54

[136] R. Krall, F. Y. Cyr-Racine and C. Dvorkin, JCAP **1709**, no. 09, 003 (2017) doi:10.1088/1475-7516/2017/09/003 [arXiv:1705.08894 [astro-ph.CO]]. 55

[137] M. Garny, T. Konstandin, L. Sagunski and S. Tulin, JCAP **1809**, no. 09, 011 (2018) doi:10.1088/1475-7516/2018/09/011 [arXiv:1805.12203 [astro-ph.CO]]. 55

[138] A. D. Rivero, C. Dvorkin, F. Y. Cyr-Racine, J. Zavala and M. Vogelsberger, arXiv:1809.00004 [astro-ph.CO]. 55

[139] J. Fan, A. Katz, L. Randall and M. Reece, Phys. Dark Univ. **2**, 139 (2013) doi:10.1016/j.dark.2013.07.001 [arXiv:1303.1521 [astro-ph.CO]]. 57

[140] Gaia Collaboration, Prusti, T., de Bruijne, J. H. J., et al. (2016), A&A, 595, A1 57

[141] K. Schutz, T. Lin, B. R. Safdi and C. L. Wu, Phys. Rev. Lett. **121**, no. 8, 081101 (2018) doi:10.1103/PhysRevLett.121.081101 [arXiv:1711.03103 [astro-ph.GA]]. 57

[142] J. Buch, J. S. C. Leung and J. Fan, arXiv:1808.05603 [astro-ph.GA]. 57